Gut Microbiota-derived 3-hydroxybutyrate blocks GPR43-mediated IL6 signaling to ameliorate radiation proctopathy

Zhenhuang Ge
Sun Yat-sen University https://orcid.org/0000-0002-1189-7285
Chun Chen
Shanghai Jiao Tong University
Junyi Chen
Sun Yat-sen University
Zhou Jiang
Sun Yat-sen University
Lingming Chen
Guangdong Medical University
Yingqi Wei
Sun Yat-sen University
Haiyang Chen
Sun Yat-sen University
Huaiming Wang
Sun Yat-sen University
Hui Wang
Sun Yat-sen University
Yong-jun Lu (luyj@mail.sysu.edu.cn)
Sun Yat-sen University https://orcid.org/0000-0002-3030-5724

Article

Keywords: Radiation proctopathy, 3HB, IL6, GPR43, Akkermansia muciniphila, Radioprotection

Posted Date: January 9th, 2023

DOI: https://doi.org/10.21203/rs.3.rs-2404105/v1

Additional Declarations: There is **NO** Competing Interest.

Gut Microbiota-derived 3-hydroxybutyrate blocks GPR43-mediated IL6 signaling to ameliorate radiation proctopathy

Zhenhuang Ge[1], Chun Chen[2,3], Junyi Chen[1], Zhou Jiang[1], Lingming Chen[4], Yingqi Wei[2], Haiyang Chen[5], Huaiming Wang[2,6*], Hui Wang[2,6*] and Yongjun Lu[1*]

Affiliation:

[1] Run Ze Laboratory for Gastrointestinal Microbiome Study, School of Life Sciences, Sun Yat-sen University, Guangzhou, 510275, China.

[2] Department of Colorectal Surgery, The Sixth Affiliated Hospital, Sun Yat-sen University, Guangzhou, 510655, China.

[3] Present address: Shanghai General Hospital, School of Medicine, Shanghai Jiao Tong University, Shanghai, 201620, China.

[4] School of Medical Technology, Guangdong Medical University, Dongguan, 523808, China.

[5] Department of Radiation Oncology, The Sixth Affiliated Hospital, Sun Yat-sen University, Guangzhou, 510655, China.

[6] Guangdong Institute of Gastroenterology, Guangdong Provincial Key Laboratory of Colorectal and Pelvic Floor Diseases, Supported by National Key Clinical Discipline, Guangzhou, 510655, China.

*** Corresponding authors**

Dr. Yongjun Lu, Run Ze Laboratory for Gastrointestinal Microbiome Study, School of Life Sciences, Sun Yat-sen University, Guangzhou, China. Tel: 86-020-84110778. Fax: 86-020-84036215. e-mail: luyj@mail.sysu.edu.cn.

Dr. Hui Wang, Department of Colorectal Surgery, The Sixth Affiliated Hospital, Sun Yat-sen University, Guangzhou, 510655, China. e-mail: wang89@mail.sysu.cn.

Dr. Huaiming Wang, Department of Colorectal Surgery, The Sixth Affiliated Hospital, Sun Yat-sen University, Guangzhou, 510655, China. e-mail: wanghm7@mail.sysu.edu.cn.

ABSTRACT

Radiation proctopathy (RP) is a common complication of pelvic radiotherapy but lacking effective treatment. RP accompanies by microbial dysbiosis. However, how the gut microbiota affects the disease remains unclear. Here, we reveal that the fecal and serous concentrations of microbiota-derived 3-hydroxybutyrate (3HB) are significantly reduced in RP mice and radiotherapeutic patients. Moreover, the concentration of 3HB is negatively associated with the expression of proinflammatory IL6 that is increased along with the severity of radiation damage. 3HB treatment significantly downregulates IL6 expression and alleviates IL6-mediated radiation damage. Such a radioprotection of 3HB is mediated by GPR43. *Akkermansia muciniphila*, with a significant reduction in RP mice and patients, is associated with lower 3HB concentration. Treatment of *A. muciniphila* significantly increases 3HB concentration, downregulates GPR43 and IL6 expression, and ameliorates radiation damage in mice. Collectively, these results demonstrate that the gut microbiota, including *A. muciniphila*, induce higher concentrations of 3HB to block the GPR43-mediated IL6 signaling, thereby conferring radioprotection in RP mice. Our findings reveal a novel implication of the gut-immune axis in radiation pathophysiology, with potential therapeutic applications.

Keywords: Radiation proctopathy, 3HB, IL6, GPR43, *Akkermansia muciniphila*, Radioprotection

Introduction

For decades, radiotherapy has been an important component of both curative and palliative care for cancer patients, but it is also associated with serious unfavorable side effects.[1] The intestine is a major target of radiotherapy. Radiation-induced intestinal injury is a serious comorbidity that affects cancer patients and remains a long-standing and unresolved problem. Long-term radiation-induced intestinal adverse effects now outnumber ulcerative colitis and Crohn's disease in terms of prevalence.[2] The intestine is the largest niche for gut microbiota. Clinical evidence shows that the gut microbiota changes during radiotherapy and is associated with radiation enteropathy.[3, 4] Although there are sporadic descriptive studies demonstrating associations between damage caused by radiation enteropathy and the gut microbiota,[1] the causal link with disease activity has not yet been established. In addition, despite decades of rigorous research, medical intervention to prevent radiation harm is still a global challenge.

Radiation proctopathy (RP), a frequent side effect of radiation therapy for pelvic malignancies (such as tumors of the bladder, testes, prostate, rectum, cervix, and uterus) with high incidence (more than 75% of patients after radiotherapy have RP symptoms), is characterized by inflammation of colon tissue; however, there is no effective treatment available.[5] Currently, clinical care of RP is difficult due to the lack of recommendations or standard therapy regimens; thus, the clinical outcomes of chronic RP are poor. Moreover, the fundamental mechanism behind RP development and advancement is still unknown, demanding additional research on RP pathogenesis, progression, and treatment.[5, 6]

Although we now know that epithelial injury, the immune system, and the gut microbiota are involved in the pathogenesis of radiation enteropathy,[2, 7-9] their

interaction needs to be investigated further. Growing evidence points to the gut microbiota's critical role in the onset of radiation-induced damage. Recently, it was shown in a mouse model for the first time that radiation-induced dysbiosis has the pathogenic ability to cause bowel injury, shedding light on the alterations in the microbiome can affect bowel damage.[10] Another study demonstrated the beneficial role of fecal transplantation in treating mice with radiation-induced damage.[11] Moreover, radiation leads to inflammation and gut microbiota dysbiosis. For example, tissue damage brought on by radiation is linked to higher levels of cytokine expression (e.g., interleukin (IL)1β, IL6) in both human and mouse models.[7, 12] A large clinical study on the association of microbiota with radiation enteropathy showed that an altered microbiota is associated with the expression of intestinal mucosal cytokines.[3] These studies suggest the existence of an immunity-microbiome axis in radiation enteropathy. As gut microbial dysbiosis, which lead to aberrant immune responses, has been associated to the development of many diseases,[13, 14] it's conceivable that re-establishing the balance between microbiota and host immunity is just as critical for resolving radiation enteropathy symptoms. The clinical application of microorganisms in reducing the toxicological effects of radiation seems promising, although it is still at an early stage.[1, 2]

The physiological functions of gut microbiota and metabolic systems (including host and microbial metabolism) are critical in regulating human health and diseases.[15, 16] Metabolites produced by commensal bacteria play an important role in the host-microbiota cross talk and affect host health.[17] Growing evidence has emphasized the relevance of gut microbiota-derived metabolites in physiology and immunological homeostasis,[18] however, the characterization of metabolites and regulatory networks involved in host-microbiota interactions in RP have not yet been elucidated.

To better understand the interactions between the radiation-induced damage and the metabolites derived from gut microbiome, we aimed to use a mouse RP model and multi-omics strategies to characterize the dynamics of the gut microbiota-derived metabolites and their interplay with the host immune system, to identify and uncover the underlying mechanisms of the potential metabolites and their producing bacterium implicating in radioprotection. Our findings shed new light on the causal mechanism of the interplay between the RP damage, the gut microbiota-derived metabolites, and host immunity, which might potentially help prevention and treatment strategies of RP in the future.

Results

The concentrations of gut co-metabolite 3HB are significantly reduced in feces and serum of irradiated mice and radiotherapeutic patients.

To evaluate the impact of radiation treatment on the metabolite profiles and identify the metabolites related to tissue damage in RP, a RP-mouse model that we previously developed[19] was exposed to radiation in the pelvic area while the rest of the animal's body was protected by lead blocks (**Figure 1A**), instead of the existing models that use complete abdominal irradiation and focus mostly on radiation-induced intestinal fibrosis.[11] Hematoxylin and eosin (H&E) and Masson staining of representative lesions demonstrated that irradiation caused typical RP pathologies, such as mucosal damage, hyperplasia, submucosal thickening, and edema in the muscular layer of distal colorectal tissue (**Figure 1B**). The histopathological changes were evaluated by radiation injury score (RIS) (**Table S1**), and the results showed a significantly increased RIS score in RP mice, indicating severe tissue injury (**Figure 1C**). These

data demonstrate that this model replicates the characteristics of pathological RP in humans.[2, 6, 20, 21]

Next, we evaluated whether such radiation damage may correlate with alternations of metabolite profiles. To address this, LC-MS analysis of metabolites in sera isolated from unirradiated (UR) and RP mice was performed. Rarefaction analysis comparing metabolite diversity within individual subject revealed that RP mice harbor a clearly distinct metabolite profiles compared to UR mice (**Figure 1D**). Volcano plot analysis for all identified metabolites found 24 metabolites with significant changes ($P < 0.05$) and a confirmed variable importance (VIP score > 1) in RP mice (**Figure 1E; Figure S1A; Table S2**). Furthermore, the differential metabolites between RP and UR mice were enriched in different metabolomic signaling pathways using KEGG enrichment analysis. Among these pathways, synthesis and degradation of ketone bodies was a top one altered in mice (**Figure 1F**). Importantly, the concentrations of 3-hydroxybutyrate (3HB), a representative member in this pathway, were significant lower in serum of RP mice than UR mice (**Figure 1G; Figure S1B**). However, no significant difference of 3HB abundance was found in liver between RP and UR mice (**Figure S1C**), suggesting that the difference of 3HB concentration in serum is not regulated by liver. Notably, the cluster analysis of differentially expressed metabolites showed that most of the organic acids and their derivatives, including 3HB, are co-metabolites of gut microbiota and host (**Figure 1H**).

We next explored whether 3HB is a co-metabolite of gut bacteria and contributed significantly to the concentration of 3HB in the sera. To address this, mice were treated with broad-spectrum antibiotics for removing the bacteria from the intestine (**Figure S2**). Compared to mice drinking water only, antibiotic-treated mice with depleted intestinal microbiomes exhibited distinct metabolite composition and

reduced abundance of metabolites in feces (**Figure S3A-C**). Interestingly, organic acid and its derivatives, especially 3HB, were significantly reduced in feces of gut microbiota deficient mice compared to control (**Figure S3D-F**). These results reveal that 3HB is a gut co-metabolite derived from gut microbiota. We then analyzed the metabolites in mice sera to validate whether the differences of 3HB are due to the alterations of gut microbiota composition. The results showed that gut microbiota deficient mice harbor distinct metabolite profiles compared with control mice (**Figure S4A-C**). Remarkably, the reduced concentration of 3HB in serum is consistent with the reduction of 3HB observed in feces of gut microbiota deficient mice, and is significantly associated with the abundance of certain gut microbiota (**Figure S4D-H**). Importantly, no significant difference of concentration of 3HB was found in the liver of gut microbiota deficient and control mice (**Figure S4I**), further confirming that the altered 3HB in serum is gut derived. Altogether, these results suggest that gut microbiota-derived 3HB is an important contributor to the concentrations of 3HB in serum.

We subsequently assessed the fecal metabolite profiles of RP mice to analyze the abundance of 3HB. PCA plots revealed that metabolite profiles in feces are also very distinct between RP and UR (**Figure 1I**), and 147 metabolites were identified with significant changes and VIP scores, in which 3HB was indeed significantly decreased in RP mice (**Figure 1J-L; Figure S5A-B; Table S3**). Importantly, there was a statistically significant positive correlation between the abundance of 3HB in fecal and serum samples derived from RP mice (**Figure 1M; Figure S5C ; Table S4**). These results collectively suggested that such a reduction of 3HB in serum is caused by the decrease of 3HB in feces of RP mice. Moreover, a clinical detection of samples from patients uncovered that, compared to those before radiotherapy (BT), human

subjects after radiotherapy (RT) exhibit a significantly decreased concentrations of 3HB in both fecal and serum samples (**Figure 1N-O**), showing an association of decreased 3HB concentration with the exposure of radiation, both in mice and human subjects.

Taken together, these data demonstrated that radiation leads to the reduction of levels of gut co-metabolite 3HB, and suggest that 3HB may have radioprotective benefits.

Oral administration of 3HB ameliorates radiation-induced damage and attenuates inflammation in RP mice

Subsequently, we tested whether the increased 3HB concentration can ameliorate radiation-induced damage in RP mice. Compared to mice treated with saline, gavage of 3HB significantly increased the 3HB concentration in the feces and serum of RP mice (**Figure 2A-C**). The effects of 3HB were assessed by histological analysis. The results showed that the clinical score (encompassing the body parameters listed in Table S5 for evaluating radiation-induced damage, which have been proved to be proportional to disease severity[11]) of RP mice with 3HB treatment is significantly lower than that of those with saline treatment (**Figure 2D**). In addition, 3HB-treated mice have longer colon length and decreased rectum weight. Thus, 3HB remarkably improves the pathological damage of the colon and rectum caused by radiation, inducing a protective effect against inflammation (**Figure 2E-H**). Furthermore, histological analysis revealed that 3HB treatment also reduces crypt damage, mucosal ulceration, immune cell infiltration, and interstitial edema (**Figure 2I**), which was manifested by a marked decrease in the RIS score (**Figure 2J**).

Altogether, these data demonstrate that 3HB effectively ameliorates radiation-induced damage and benefits radioprotection of mice, suggesting that 3HB is a mediator of radioprotection.

Reduced concentration of 3HB is negatively associated with the expression of proinflammatory IL6 that increased along with disease severity

Since tissue damage of RP is associated with immune system and 3HB can significantly improve the feature of colorectal inflammatory (**Figure 2E-H**), we then further analyzed whether RP-induced injury may also correlate with the expression of certain cytokines. To this end, the tissues were collected from RP and UR mice to analyze the colonic and rectal tissue injury and inflammatory cytokine expression. The results showed that the clinical score proportional to disease severity is significantly higher in RP mice compared to UR mice (**Figure 3A**). The colon length was shorter, and the rectum was thicker with increased rectal weight in RP mice, compared to UR (**Figure 3B-E**), indicating a severe inflammation.

Thus, we subsequently assessed the expression of 10 pro- and anti-inflammatory cytokines in the sera of UR and RP mice. These cytokines were selected for analyses based on their well-known significance in modulating inflammation response and immune system regulation.[22] The expression of pro-inflammatory cytokines IL1β, IL2, IL6, and TNFα was significantly increased in RP mice, whereas that of anti-inflammatory cytokines IL4 and IL5 was significantly decreased (**Figure 3F**). However, only IL6 expression level paralleled with the severity of radiation-induced damage (**Figure 3G**), suggesting its importance in response to radiation. Additionally, compared with UR mice, RP counterparts showed higher expression levels of phosphorylated (p)-STAT3, the intracellular signaling cascade pathway activated by

IL6 expression (**Figure 3H-I**), further confirming that the IL6 signaling pathway is activated and enhanced. We then examined whether the abundance of selected differential bacteria may be correlated to abnormal inflammation status in RP mice. Interestingly, although the altered expression of six cytokines were observed in RP mice, only IL6 exhibited a stronger negative correlation to the concentration of 3HB (**Figure 3J-K**), suggesting its implication in mediating the radioprotection of 3HB. Importantly, the concentrations of IL6 were also significantly higher in serum samples from subjects post treatment (RT) than those before radiotherapy treatment (BT) in clinical oncology patients (**Figure 3L**).

Collectively, these data suggest that IL6 plays a significant role in RP development, and may involve in the modulation of radioprotection of 3HB.

Radioprotection of 3HB against RP damage is mediated by IL6 signaling

To investigate whether IL6 plays a causative role or a protective compensatory response in RP development, we tested whether inhibition of IL6 could ameliorated or worsen the effects of radiation-induced damage. To this end, mice were injected with anti-IL6 mAb or treated with IgG antibody as control (**Figure 4A**). The results showed that RP mice treated with anti-IL6 MAb have significantly lower clinical scores than those injected with saline or IgG (**Figure 4B**). Consistently, the protein abundance of pSTAT3 was also decreased in mice treated with anti-IL6 MAb (**Figure 4C**), indicating that activated IL6 signaling is weakened. In addition, treatment of IL6 receptor antagonist significantly improved the colonic length and rectal weight of RP mice (**Figure 4D-G**), indicating a reduced inflammation symptoms. Moreover, the assessment of radiation-induced tissue damage using H&E and Masson immunostaining showed that mice receiving anti-IL6 mAb treatment display fewer

lesions and a more intact mucosa, and ameliorated RIS scores (**Figure 4H-I**). Thus, these data reveal that the blockade of IL6 signaling attenuates the RP damage in mice, indicating that IL6 is a major mediator of radiation-induced RP damage.

Given the fact that IL6 is a major driver of radiation-induced tissue damage and that 3HB treatment confers the same benefits as IL6 blocking, we next investigated whether 3HB directly mediates IL6 production upon radiation treatment in mice and cell lines. Indeed, 3HB treatment significantly downregulates the expression of IL6 (**Figure 4J**) and the protein levels of pSTAT3 of rectal tissue in RP mice (**Figure S6A-B**). Furthermore, 3HB treatment also significantly downregulates IL6 expression in irradiated HIEC-6 epithelial cells compared to those treated with saline (**Figure 4K-L**). These results demonstrate that 3HB can directly downregulate the expression of radiation-induced IL6.

Collectively, these results indicate that IL6 is a major mediator of RP damage and provide evidence that the radioprotective effect of 3HB against RP damage is partially ascribed to the regulation of IL6 expression.

3HB exerts radioprotective effect against RP damage *via* GPR43

We further explored how 3HB regulates IL6 expression. We therefore performed KEGG enrichment analysis of the differentially expressed metabolites in sera and feces between RP and UR mice, respectively. The results showed that these metabolites are clustered in various pathways, in which the synthesis and degradation of ketone bodies and cAMP signaling pathways are enriched in both serum and fecal samples (**Figure 5A**). On the other hand, as 3HB can act as a signaling molecule *via* G protein-coupled receptors (GPRs) to initiate additional signaling cascades,[23] including the cAMP signaling pathway (**Figure 5A**), we next investigated whether

306 and which GPRs mediate the radioprotective role of 3HB. GPR43, GPR41, GPR109A,
307 GPR81, GPR35, and GPR40 were selected for analysis based on their well-
308 established importance in mediating immune and metabolic functions.[24] We found
309 that, compared with UR mice, the expression of *GPR43*, but not other GPRs, in RP
310 mice is significantly increased in colorectal tissues (**Figure 5B-C**). Furthermore, the
311 expression of *GPR43* in both colonic and rectal samples from RP mice treated with
312 3HB was significantly reduced, compared to that in untreated controls (**Figure 5D-E**).
313 These results indicated that amelioration of radiation-induced damage by 3HB is
314 associated with downregulated expression of GPR43.

315 Given that 3HB decreases the expression level of IL6, we wanted to identify the
316 transcriptional regulator of IL6 regulated by 3HB. To address this, we initially
317 assessed the expression of *il6* mRNA in colorectal tissue of RP and UR mice. As
318 expected, the levels of *il6* mRNA are significantly higher in colonic and rectal
319 samples from RP mice than those from UR mice (**Figure S7A**). A number of known
320 transcription factors that have been shown to regulate IL6 gene transcription were
321 selected for analysis.[25] The results showed that compared with UR mice, the
322 expression of SP1, but not other regulators, in RP mice is both significantly increased
323 in colonic and rectal tissues (**Figure S7B**). Indeed, RP mice treated with 3HB
324 significantly reduced the expression of *sp1* and *il6* in both colonic and rectal samples,
325 compared to that in untreated controls (**Figure S7C-D**). These results indicated that
326 3HB inhibits radiation-induced IL6 expression *via* transcriptional regulator SP1.

327 We subsequently tested whether GPR43 is involved in the regulation of SP1 using
328 the irradiated cell model and co-culture experiment. The results showed that SP1
329 inhibitor significantly downregulates the expression of *sp1* and *il6*, but not *gpr43* in
330 irradiated cells (**Figure S7E-G**). Remarkably, with or without 3HB co-treatment,

GPR43-synthetic agonist increased the expression of *il6* and *sp1*, compared to 3HB treatment alone, in irradiated cells (**Figure 5F; Figure S7H**). These results not only confirmed a direct role of SP1 in regulation of radiation-induced IL6 but also indicated the control of GPR43 on SP1. Moreover, the downregulation of IL6 by 3HB was blocked by GPR43 agonist, in which 3HB treatment significantly downregulated the expression of IL6 while the co-treatment with GPR43 agonist blocked the function of 3HB (**Figure 5F**). Notably, these results are in consistent with those *in vivo* analyses in mice, indicating that the inhibition of 3HB on radiation-induced IL6 expression was mediated by GPR43.

We next investigated whether GPR43 agonist impairs the radioprotective effect of 3HB in RP mice. RP mice pre-treated with antibiotics were treated with or without 3HB and GPR43 agonist (**Figure 5G**). The results showed that, compared with those of controls, GPR43 agonist treatment significantly suppressed the effects of 3HB in downregulating the expression of IL6, reducing pSTAT3 levels, and ameliorating clinical scores (**Figure 5H-I**; **Figure S6C-D**). Consistently, compared with controls, treatment of GPR43 agonist prevented the protective effects of 3HB on radiation-induced pathological damage of the colonic and rectal tissues (**Figure 5J-M**). In addition, histological analysis revealed that the GPR43 agonist impairs the effects of 3HB in reducing damage of crypts, mucosal ulceration, immune cell infiltration, and interstitial edema, resulting in a high RIS score with no statistical significance compared to the controls (**Figure 5N-O**). Thus, blockage of the radioprotection of 3HB by activating GPR43 indicates GPR43 as a major mediator of 3HB against RP damage in mice.

Taken together, these results demonstrate that GPR43 mediates the radioprotection of 3HB by downregulating the expression of IL6 during radiation-induced RP progression.

Gut bacterium *Akkermansia muciniphila* promotes 3HB concentration and downregulates the radiation-induced IL6 expression

Since gut but not liver involved in the alteration of the serous 3HB concentration in RP mice, we hypothesized that the gut microbiota may contribute to control the level of 3HB concentration. To address this, we performed 16S rDNA sequencing of fecal samples to analyze the composition of the gut bacteria in UR and RP mice. Principal co-ordinates analysis (PCoA) revealed that RP mice harbor a distinct bacterial community relative to UR mice (**Figure 6A**). Compared to UR, the abundance of Firmicutes and Bacteroidetes were reduced and the abundance of Proteobacteria was increased in RP mice. In particular, Verrucomicrobia, and a representative species of Verrucomicrobia, *Akkermansia muciniphila*, were significantly reduced in RP mice (**Figure 6B-C**). LEfSe was utilized to identify the bacterial taxa linked to radiation-induced tissue injury. A total of 14 dominant bacteria showed a significant change in abundance in RP mice compared with UR mice (LDA score > 3, $p < 0.05$), among which *A. muciniphila* was the most significantly reduced species post radiation (**Figure 6D**). Additionally, random forest analysis showed that *A. muciniphila* displays a high Gini score, further confirming its role in RP development (**Figure 6E**). Notably, a decrease in the abundance of *A. muciniphila* in the features of radiation-reshaped gut microbiota was consistent with that reported in previous study.[11] We then evaluated the association between 3HB concentration and the significantly changed bacteria in RP mice to find dominant bacteria that can enrich 3HB

concentration. We found that the reduction of 3HB concentration induced by radiation is significantly correlated with the decrease of the abundance of *A. muciniphila* in RP mice (**Figure 6F-G; Table S6**). Meanwhile, mice with depleted intestinal microbiomes were used to find the bacteria that play dominant effects on the changes of 3HB concentration in feces under normal conditions. The results revealed significant correlations between the dominant bacteria with reduced abundance and six gut co-metabolites with decreased concentration, and uncovered that *A. muciniphila* abundance is positively correlated with 3HB concentration (**Figure S8**). Therefore, these results collectively suggest that a radiation-induced decrease of the abundance of *A. muciniphila* led to the reduction of 3HB concentration.

We thus measured the concentration of 3HB in the culture supernatant at different time points based on the growth curve of *A. muciniphila* to validate whether *A. muciniphila* can produce and promote the accumulation of 3HB. The results showed that the concentration of 3HB increased during the growth phases of *A. muciniphila*, with much higher concentrations during the stationary phase (**Figure 6H-I**). Moreover, Kyoto Encyclopedia of Genes and Genomes (KEGG) analysis and previous studies showed that FabG might be involved in the biosynthesis of 3HB,[26, 27] and the presence of an expressible *fabG* gene in *A. muciniphila* was confirmed by PCR and qPCR analyses, respectively (**Figure S9A-B**). When treated with epigallocatechin gallate (EGCG), an inhibitor of FabG,[28] the 3HB concentration in the culture supernatant of the bacteria in stationary phase was decreased with a EGCG concentration dependent manner, whereas the survival and growth rate of *A. muciniphila* did not affect (**Figure S9C-D**), further confirming that *A. muciniphila* can produce and accumulate 3HB. Furthermore, gavage of *A. muciniphila* significantly increased fecal and serous 3HB concentrations in the RP mice (**Figure**

404 **6J-L**). Thus, these data collectively indicate that gut *A. muciniphila* is an important
405 contributor to affect 3HB levels in RP mice.

406 Next, we tested whether *A. muciniphila* can play a role in the regulation of
407 radiation-induced IL6 expression. The irradiated cells treated with live but not heat-
408 inactivated *A. muciniphila*, result in significant downregulation of the expression of
409 IL6 (**Figure 6M**). To further investigate the contribution of *A. muciniphila* and post-
410 radiation microbiota to IL6 expression, an *in vitro* epithelial cell co-culture model was
411 utilized. IL6 level was higher in the irradiated cells treated with fecal suspensions
412 derived from RP mice than those treated with that derived from UR mice. Moreover,
413 supplementation of live but not inactivated *A. muciniphila* into the microbiota derived
414 from RP mice significantly reduced IL6 expression in co-cultured irradiated cells
415 (**Figure 6N**). We also studied whether GPR43 is involved in the downregulation of
416 IL6 expression by *A. muciniphila* treatment. Compared with controls, *A. muciniphila*
417 treatment significantly downregulated IL6 expression, whereas *A. muciniphila* plus
418 the GPR43 agonist blocked the decrease of IL6 expression (**Figure 6O**). Therefore, *A.*
419 *muciniphila* can directly downregulate radiation-induced expression of IL6 *via*
420 GPR43-mediated pathway.

421 Moreover, in RP mice, the abundance of *A. muciniphila* was positively correlated
422 with most of the bacteria that decrease in abundance but negatively correlated with
423 most of the bacteria that increase in abundance (**Figure S10A; Table S7**), and was
424 also negatively correlated with the expression level of IL6 (**Figure S10B; Table S8**).
425 Importantly, like the results from mice, the abundance of fecal *A. muciniphila* was
426 significantly lower in clinical oncology patients after radiotherapy treatment (BT)
427 than those before treatment (RT) (**Figure 6P**). These results indicate that decreased *A.*

muciniphila levels are related to radiation injury, and suggest that gavage of *A. mucinihila* may provide radiation protection.

Taken together, these results demonstrate that *A. muciniphila*, an important contributor of 3HB levels, can also downregulate IL6 expression through GPR43-mediated pathway, suggesting a potential radioprotective benefits for RP.

Gavage of *A. muciniphila* increases 3HB concentration, reduces IL6 expression and ameliorates radiation-induced damage in RP mice

We then investigated whether *A. muciniphila* can confer radioprotective effects against RP in mice. To address this, RP mice pre-treated with antibiotics were orally administered *A. muciniphila* or saline (**Figure 7A**). Fluorescence *in situ* hybridization (FISH) analysis by using an *A. muciniphila*-specific probe showed that *A. muciniphila* cells colonize the intestinal epithelium of mice fed with *A. muciniphila*, compared with saline-treated mice (**Figure 7B**). Colonization of *A. muciniphila* in colonic mucosa were also observed by transmission electron microscopy (**Figure S11**). Furthermore, the increased colonization of *A. muciniphila* was confirmed using *A. muciniphila*-specific qPCR (**Figure 7C**). These results indicate that *A. muciniphila* indeed can colonize in intestinal compartment upon gavage.

Notably, gavage of *A. muciniphila* significantly increased the fecal and serous 3HB concentrations in the mice (**Figure 7D-E**). The expression of *GPR43* in both colonic and rectal samples from RP mice treated with *A. muciniphila* was also significantly reduced, compared to that in untreated controls (**Figure 7F-G**). Indeed, compared to mice fed with saline, mice fed with *A. muciniphila* resulted in downregulated expression of IL6 and pSTAT3 in rectal tissues and lower clinical scores (**Figure 7H-I; Figure S6E-F**). As expected, *A. muciniphila* treatment significantly prevented

shortening of colonic length and thickening of rectal tissue (**Figure 7J-M**). Moreover, pathological and histological analyses showed that gavage of *A. muciniphila* remarkably protects the distal colorectal tissue from radiation-induced damage, and reduced damage to crypts, mucosal ulceration, immune cell infiltration, and interstitial edema (**Figure 7N**), which was manifested by a marked decrease in the RIS score (**Figure 7O**). Thus, these results reveal that *A. muciniphila* confers radioprotective effects on radiation-induced RP damage by increasing the fecal and serous 3HB concentration, downregulating the expression of GPR43 and IL6.

Discussion

Increasing evidence has highlighted that immune system and the gut microbiota are involved in the pathogenesis of RP,[2, 7-9] and that metabolites produced by commensal bacteria play an important role in the host-microbiota cross-talk. However, the relevance and characterization of regulation between gut microbiota and metabolomic involved in physiology and immunological homeostasis of RP have not yet been elucidated. This study demonstrated that dysbiosis and abnormal status of metabolic systems (including host and microbial metabolism) induced by radiation are associated with the pathogenesis of RP, as evidenced by the fact that the regulation of gut microbiome-metabolome network and its interaction with the immune system can provide significant protection against post-radiation tissue damage in mice.

Our study showed that the metabolite profiles of RP mice is characterized by significant reduced concentration of 3HB, a gut co-metabolite derived from commensal bacteria, higher levels of IL6, and severe tissue damage. We further provided evidence that gut microbiota-derived 3HB plays a radioprotective role in intestinal inflammation and tissue damage. Mechanistically, gavage of 3HB

significantly ameliorates radiation-induced damage by downregulating GPR43-mediated IL6 expression in RP mice. Moreover, our study showed that the gut microbiome pattern of RP mice is characterized by the reduction of core species, particularly *A. muciniphila* which serves as an important contributor for 3HB concentration. We confirmed that gavage of *A. muciniphila* increases 3HB concentration of mice and contributes substantially to radioprotection. Our findings contribute to advance our knowledge of the link between the RP disease mechanism and gut microbiome, and provide potential prevention and treatment for alleviating clinical radiation-induced damage.

Radiation therapy is employed in at least 50% of cancer patients, particularly for the treatment of urological, gynecological, and rectal malignancies in the pelvic region,[2] but a lot of them experience long-term morbidity from RP, which significantly lowers their life quality.[20, 29] Over the past few decades, cancer incidence and death have changed just slightly, but the number of cancer survivors has increased by roughly three times during the same period. Thus, in the future, it is anticipated that the worldwide burden of RP would significantly increase.[2] Given that more than 75% of the patients who receive radiotherapy have RP symptoms, our clinical data that radiotherapy treatment causes decreased *A. muciniphila* abundance, reduced 3HB concentration and increased IL6 level in patients may help to indicate the degree of risk of RP. On the other hand, the knowledge of RP pathogenesis and treatment options remain limited.[30] Thus, a deeper comprehension of the disease's mechanism is urgently required for developing efficient therapies.

As an initial step of this study, we attempted to identify the metabolites and inflammatory cytokines linking to the pathogenesis of RP. Our results demonstrated that radiation can alter the fecal and serous metabolite profiles of RP mice, in which

503 the concentration of 3HB is significantly reduced. Radiation also increases the
504 expression of inflammatory cytokine IL6 that exhibits significant negative correlation
505 with 3HB. Previous study[12] and our results show that the expression of IL6 is
506 correlated with the severity of radiation-induced damage and therefore is a good
507 marker of RP. Although 3HB has been shown to have significant therapeutic effects
508 in colitis and colorectal cancer,[31, 32] it remains unknown whether 3HB serves as an
509 immune effector. We confirmed that 3HB directly downregulates radiation-induced
510 IL6 expression and exerts a radioprotective effect. This result is also be supported by
511 a previous study demonstrating that treatment with 3HB suppresses the levels of
512 inflammatory cytokines IL1β, IL6, and IL8 in human placental tissue culture.[33]
513 Another study reported that 3HB reduced NLRP3 inflammasome-mediated IL1β and
514 IL18 production in human monocytes.[34] These findings suggest that 3HB is an
515 immune effector and may be a promising mediator of radioprotection. In addition to
516 3HB, we also identified other metabolites whose levels were reduced in RP mice.
517 Further studies are required to investigate whether these compounds have
518 radioprotective properties.

519 The current data using our RP mouse model demonstrated that irradiation leads to
520 dysbiosis, which is consistent with previous findings.[7-9] Alterations in intestinal
521 microbiota were observed in patients with RP, but a causal association with disease
522 activity has yet to be established.[1] Our research revealed for the first time that
523 radiation treatment impairs colonization and abundance of *A. muciniphila*. In addition,
524 the current study shows that the abundance of *A. muciniphila* is positively correlated
525 with the concentration of 3HB in fecal and serous samples from RP mice, and both *in*
526 *vitro* and *in vivo* experiments confirmed that *A. muciniphila* exhibits a dominant role
527 in mediating the accumulation of 3HB. Therefore, at least one of the radioprotective

528 pathways of *A. muciniphila* may be achieved by mediating the accumulation of 3HB.
529 Moreover, other metabolites derived from *A. muciniphila* are known to attenuate
530 proinflammatory cytokine responses.[35, 36] Therefore, identifying more effective
531 metabolites may provide a comprehensive understanding of the pleiotropic effects of
532 *A. muciniphila* on radioprotection.

533 *In vitro* findings in the current study demonstrated that *A. muciniphila* has a direct
534 down-regulation effect on the expression of IL6 in epithelial cell line. Thus, *A.*
535 *muciniphila* plays a protective role in intestinal inflammation and tissue damage, at
536 least in part through the increase of 3HB concentration and the reduction of IL6 level.
537 Previous studies have shown that lack or decrease in the abundance of *A. muciniphila*
538 is linked to many diseases, including steatosis of the liver, inflammation, obesity,
539 diabetes, and the response to cancer immunotherapies.[37] Our data added a novel and
540 effective application for *A. muciniphila* in RP treatment.

541 Our finding on the function of GPR43 has a potential clinical relevance. Previous
542 studies have shown that GPR43 is extensively expressed in immune tissues and
543 cells,[38] suggesting its important role in immune responses. However, the role of
544 GPR43 in the inflammatory response remains elusive. GPR43 may have both pro- and
545 anti-inflammatory effects, depending on the disease model employed.[39-43] In addition,
546 GPR43 may mediate interactions between the human host and gut microbiome.[44] Our
547 results demonstrated that activation of GPR43 blocks the downregulation of IL6 by *A.*
548 *muciniphila* or *A. muciniphila*-mediated 3HB and prevents the radioprotection, further
549 pointing to the unique association of GPR43 with gut microbiota and radiation-
550 induced IL6 expression in the pathogenesis of RP. The relationship between GPR43
551 and IL6 has also been reported in other studies. For example, knockout of GPR43
552 reduces IL6/IL1β/TNFα levels in cells transfected with *Klebsiella pneumoniae*.[45]

553 Another study found that GPR43 activation enhances psoriasis-like inflammation by
554 upregulating IL6 signaling in the epidermis.[46] These findings suggest that GPR43 may
555 also play a crucial role in radiation-induced intestinal injury. Our results will be
556 particularly relevant for the clinical application of GPR43 agonists or antagonists in
557 patients with RP. Therefore, future clinical trials are needed to evaluate the inhibition
558 effect of GPR43 signaling in patients with RP.

559 Gut microbiota may be useful for the prevention and treatment of RP. We showed
560 that RP mice has depletion in the Firmicutes and Bacteroidetes phyla and an increase
561 in Proteobacteria, similar to what was observed in inflammatory bowel disease
562 (IBD).[47] Thus, dysbiosis is a common feature in IBD and RP. Moreover, we found
563 that RP and IBD share similarities, as both are accompanied by fibrosis, inflammation,
564 epithelial barrier breaches, and mucosal immune cell infiltration. Modulation of IBD
565 activity by manipulating the microbiome is now gaining a lot of attention, thus it
566 seems sense for RP to follow suit. Probiotics, certain diets, and fecal microbial
567 transplants (FMT) have all been recommended for the treatment of IBD and may also
568 be effective for the management of RP. Attempts at bacteriotherapy in the setting of
569 RP appear to be safe, according to several research conducted on both rodents and
570 humans.[48, 49]

571 In conclusion, the results of this study demonstrate radiation-induced changes in the
572 microbiome and metabolome and how such an alteration impacts RP-induced
573 inflammation and RP progression. These findings suggest the potential of *A.*
574 *muciniphila* and 3HB in the treatment of RP, and that effective treatment of RP could
575 be achieved by modulating the gut microbiota and its interaction with the immune
576 system. Collectively, given the fact that current therapeutic methods for remission of

the adverse side effects of RP are limited and expensive, our study provides a promising clinical option for the management of the damage associated with RP.

Materials and methods

Mice

Female C57BL/6J mice aged 6-8 weeks were kept in a specified pathogen-free (SPF) environment with unrestricted access to drinking water and food under temperature-controlled settings and a 12-hour light/dark cycle. The littermates were used in the experiments. All animal research was approved by the Institutional Animal Care and Use Committee of the Sixth Affiliated Hospital, Sun Yat-sen University (IACUC-20200813).

RP mouse model

The mice were treated with rectal radiation using an RS2000 device (Rad Source, USA) as we previously described.[19] The mice were subjected to irradiation (25 Gy; 2.14 Gy/min) while being protected by a 4 mm thick lead shelter that exposed the lower pelvic area (1 cm^2) including the rectum in the centre of the field. After irradiation, the mice were kept in an SPF setting with regular feed and water. Unless otherwise specified, mice were examined for changes in body weight and other bodily parameters 8 weeks following radiation. Clinical scores were calculated based on weight reduction, physical appearance, posture, mobility, anal hair, and hydration using a minor modified cumulative scoring method (Table S5).[11]

Clinical oncology patients

Human fecal and serum samples were obtained from 7 rectal cancer patients before and after treatment of radiotherapy, which is recommended by National Comprehensive Cancer Network. The detailed information of the oncology patients was showed in table S9. The experiment was approved by the internal review and the ethics boards of Ethics Committee of the Sixth Affiliated Hospital of Sun Yat sen University (2021ZSLYEC-262) with patient informed consent.

627 **Sample collection**

628 Fecal samples were collected at 8 weeks post-radiation. Samples from each animal
629 were either preserved at -80°C for microbiota composition analyses, metabolite
630 profiles, or processed for subsequent investigations. To do this, the samples were
631 combined by vortexing, homogenized in saline, then centrifuged at 800 rpm for 5
632 minutes to pellet bacterial cells. Pellets were washed in PBS, reconstituted in an
633 equivalent volume of brain-heart infusion (BHI) liquid media (with 50% glycerol),
634 and kept at -80°C for co-culture investigations. Mice in the radiation, control, and
635 treatment groups were put to death eight weeks after being exposed to radiation.
636 Blood was collected, centrifuged for 10 min at 3000 rpm after being held at ambient
637 temperature for 30 min. The supernatant serum was kept at -80°C for metabolite
638 profiles and cytokine assays. Colonic segments were promptly frozen in liquid
639 nitrogen and kept at -80°C. The rectal tissue 1 cm above the anus was excised,
640 washed, and sliced into two equal length specimens along the craniocaudal axis. For
641 western blotting or quantitative PCR, one specimen was preserved in liquid nitrogen;
642 for histopathological investigation, the second specimen was fixed in 4%
643 formaldehyde.

644 **Histopathological analysis**

645 Rectal samples, fixed in 4% formaldehyde, were used for hematoxylin and eosin (HE)
646 and Masson's trichrome staining. Sections of the tissues that were four microns thick
647 were cut using a rotary microtome (Leica, Germany), placed on slides for staining and
648 then examined under a light microscope in accordance with established techniques
649 (DM2500, Leica). A certified pathologist double-blindedly carried out histological
650 examinations. Collagen, cell nuclei, and cytoplasm received blue, dark purple, and
651 red/pink, respectively, colors in the Masson's trichrome staining. After microscopic

652 analysis of the stained slides, the radiation injury score (RIS), which was modified
653 from Langberg et al.,[50] was computed to assess the histological alterations. Such
654 changes were based on Masson and HE staining, which revealed typical histological
655 characteristics of RP lesions, including mucosal ulceration, infiltrating inflammatory
656 cells, edema, vessel stenosis, and submucosal fibrosis (Table S1).

657 **Cytokines assay**

658 The circulating concentrations of IFNγ, IL10, IL12p70, IL1β, IL2, IL4, IL5, IL6,
659 KC/GRO, and TNFα were measured using the MSD V-Plex Proinflammatory Panel 1
660 Mouse Kit (Meso Scale Diagnostics, Cat# K15048D). Serum cytokine IL6 level was
661 measured using an ELISA kit (Cloud-Clone Corp, SEA079Mu) as directed by the
662 manufacturer's instructions.

663 **Fecal 16S rDNA gene sequencing**

664 Fecal sample preparation and 16S rDNA gene sequencing were carried out as we
665 previously described.[35, 36] The QIAamp Fast DNA stool Mini Kit (Qiagen, Cat#
666 51604) was used to extract bacterial DNA from fecal samples in accordance with the
667 manufacturer's instructions. By utilizing barcoded primer pairs that targeted the V3-
668 V4 region of the 16S rDNA gene, fecal DNA samples were amplified by polymerase
669 chain reaction (PCR). The Illumina NovaSeq6000 was used to sequence the PCR
670 amplicons (Novogene Co., Ltd., China) based on standard protocols. QIIME (version
671 1.9.1) was used to examine the resultant bacterial sequence fragments. The 16S rDNA
672 variable region primers used to target the region's V3-V4 were listed in Table S10.
673 The raw sequences were saved in the Sequence Read Archive
674 (http://www.ncbinlm.nih.gov/sra).

675 Principal co-ordinates analysis (PCoA) plots were used to show the generated
676 matrices. Heatmaps among gut microbiota, cytokines and metabolite results were

created with the statistical computing environment R's 'heatmap' function. The effect size (LEfSe) of linear discriminant analysis (LDA) was utilized to find changes in relative abundance. The Spearman's correlation coefficient was used to calculate correlations. Random forest analysis was performed using the R Studio (v 3.5.0).

Immunoblot analysis

Immunoblotting was carried out as we previously reported.[35] Briefly, rectal tissues collected from the indicated mice were lysed, and total protein was isolated and measured. Extracted proteins were electrophoresed in 10% SDS-PAGE with loading buffer before being transferred to PVDF membranes (Bio-Rad) and then put in 5% fat-free milk to block for one hour. The membranes were treated with primary antibodies overnight at 4°C before being incubated for 1 hour at room temperature with a secondary antibody (Cell Signaling). The protein bands were visualized using an ECL kit (Millipore). Images were captured using a Tanon5200 machine (Tanon, China). ImageJ 1.43 software was used to analyze the data.

Antibodies

Rabbit-signal transducer and activator of transcription 3 (STAT3) (#4904, Cell Signaling), rabbit-phosphorylated p-STAT3 (#9145, Cell Signaling), rabbit-glyceraldehyde-3-phosphate dehydrogenase (GAPDH) (#5174, Cell Signaling), HRP-linked anti-rabbit IgG antibody (#7074, Cell Signaling), anti-IL6 MAb Tocilizumab (HY-P9917, MCE), and isotype control IgG (HY-P70251, MCE) were used in the study.

IL6 receptor antagonist treatment

Two weeks post-irradiation of RP mice, the animals were injected with 5 mg/kg anti-IL6 MAb, IgG antibody control, or saline every two days per week for six weeks. The clinical score plots and samples were then collected.

Co-culture of epithelial cells with microbiota

Human HIEC-6 intestinal epithelial cell line was obtained from the American Type Culture Collection and cultured in Dulbecco's modified Eagle's medium (11965092, Gibco) with 10% fetal bovine serum (12483020, Gibco) at 37°C in 5% CO_2 and 95% air for 24 h. The HIEC-6 cells were irradiated (8 Gy) using an RS2000 device. For the co-culture experiments, the epithelial cells were seeded (5×10^5 cells) into Nunc EasYFlask (25 cm^2) (Thermo Scientific), and then the medium was changed and the bacterial cell suspensions (OD_{600} of 0.5) obtained from irradiated and un-irradiated mice were added. For irradiated cells treated with *A. muciniphila*, 0.5 optical density at 600 nm (OD_{600}) of active or pasteurized inactivated *A. muciniphila* were added alone or added to the bacterial cell suspension at a ratio of 2%. Co-cultures were kept in a microaerophilic environment for 24 hours at 37°C.

RNA extraction and real-time PCR

TRIzol reagent (Takara, Japan) was used to extract total RNA from tissues or cells, and a Nanodrop spectrometer was used to measure total RNA concentration. Using a Promega cDNA Synthesis Kit, first-strand cDNA was created by following the manufacturer's instructions. To measure the expression of IL6 and GPR43, quantitative real-time PCR was carried out in triplicate using SYBR Green. The endogenous control GADPH was utilized to standardize gene expression. The primers used for IL6, GPR43, and GAPDH are listed in Table S10. The data were evaluated using an ABI StepOnePlus real-time PCR system (Applied Biosystems).

Liquid culture of *A. muciniphila*

A. muciniphila (ATCC BAA-835) was cultured in BHI medium at 37°C under anaerobic conditions, as we previously described.[36] The growth curve of *A. muciniphila* was established and the OD_{600} was measured every 12 h using a Genesys

spectrophotometer (Thermo Scientific). For detecting the effects of FabG on 3HB concentration, stationary phase grown *A. muciniphila* cells were given escalating doses of epigallocatechin gallate (EGCG) for 24 h as previously reported.[28] For gut colonization of mice by *A. muciniphila*, cultures were cleaned and concentrated in anaerobic saline containing 25% (v/v) glycerol under anaerobic conditions. In addition, an equivalent amount of *A. muciniphila* cultured in the same medium was heat-inactivated at 70°C for 30 minutes.

Antibiotics treatment

For the germ-free mice model, a mixture of ampicillin (1 mg/mL, Sigma, CAS# 7177–48-2), neomycin sulfate (1 mg/mL, Sigma, CAS# 1405–10-3), vancomycin (0.5 mg/mL, Sigma, CAS# 1404–90-6), and metronidazole (0.2 mg/mL, Sigma, CAS# 443–48-1) was added to sanitize the mice's drinking water. Three times every week, the solutions and bottles were replaced. UR mice were drinked with antibiotics mixture or water for 8 weeks. RP mice were drinked with antibiotics mixture for 1 week after two weeks of radiation, and then treated with *A. muciniphila* or 3HB for another 5 weeks. Fecal pellets were cultivated on blood agar plates, resuspended in BHI + 50% glycerol (0.1 g/mL), and incubated for 48 hours at 37°C in both aerobic and anaerobic conditions to test antibiotic sensitivity.

***A. muciniphila* oral administration**

For the treatment of mice using *A. muciniphila*, the cells were grown in BHI broth medium at 37°C under anaerobic conditions, as we previously reported.[35, 36] Gut colonization of antibiotics pre-treated RP mice by *A. muciniphila* was conducted by oral gavage with 200 μL bacterial suspension containing 2×10^8 cells or saline 3 times per week. Clinical score plots and samples were collected after five weeks of treatment.

752 **Detection of *A. muciniphila***

753 According to our previous investigation, the abundance of *A. muciniphila* in fecal
754 samples was evaluated using quantitative PCR (qPCR).[35] Following the
755 manufacturer's instructions, genomic DNA was extracted from tissues or feces using
756 the QIAamp DNA Tissue or Stools Mini Kit (Qiagen). SYBR Green-based targeted
757 qPCR devices were used. Primers as previously described were utilized.

758 **Fluorescence *in situ* hybridization (FISH)**

759 Fluorescence *in situ* hybridization (FISH) and immunofluorescence of *A. muciniphila*
760 were performed as we described previously.[35] Briefly, deparaffinization was
761 performed on paraformaldehyde-fixed paraffin-embedded colon tissue slices (5 m).
762 To identify bacterial colonization, a fluorescein-labeled oligonucleotide probe
763 targeting one area of the *A. muciniphila* 16S rDNA gene was utilized. As a negative
764 control, nonspecific hybridization was detected using the non-EUB probe. *In situ*
765 hybridization was carried out at 50°C overnight. Slides were coated with ProLong®
766 Gold with DAPI (Invitrogen), sealed with coverslips, and permitted to dry overnight
767 at 4°C in the dark before being photographed using a confocal microscope (LSM 880
768 with Airyscan).

769 **Transmission electron microscopy (TEM)**

770 Transmission electron microscopy (TEM) was used to investigate *A. muciniphila*
771 colonization as we described previously.[35] Briefly, the intestinal tissues of mono-
772 colonized mice were cut into 2-3 mm cubes and promptly fixed at 4°C overnight
773 using a 0.1 M sodium cacodylate buffer containing 3% glutaraldehyde. The samples
774 were then implanted in epoxy resin after being post-fixed in a 2% osmium tetroxide
775 buffered solution. Then, the samples were processed in the manner previously
776 described. FEI Tecnai G2 Spirit BioTwin 634 was used to create electron micrographs.

3HB treatment and determination

RP mice pretreated with antibiotics were orally gavaged with 200 μL 3HB (150 mg/kg body weight) or saline 3 times per week. Clinical score plots and samples were collected after five weeks of treatment. Irradiated HIEC-6 cells, with or without 3HB (10 mM), were cultured in 5% CO_2 and 95% air conditions for 3 days, and then the expression of IL6 was assessed. 3HB in mice sera and supernatant of *A. muciniphila* was quantified using an ELISA kit (Cloud-Clone Corp, CEB022Ge), as directed by the manufacturer's instructions.

Metabolomics analysis

The samples stored at -80°C were thawed on ice. To precipitate the proteins, 300 μL of methanol were added to 100 μL of each sample, vortexed for 3 min, and remained for 10 min at room temperature. Following 20 minutes of centrifugation at 4°C of 12,000 rpm, the supernatants were analyzed by LC-MS analysis, following the manufacturer's instructions (Metware Biotechnology Co., Ltd. Wuhan).

The first- and second-order spectra obtained by mass spectrometry were qualitatively analyzed using the self-database, metware database (MWDB), and the public database of metabolite information. Multiple reaction monitoring (MRM) triple quadrupole mass spectrometry was used to quantify the metabolites. The statistical function prcomp inside R was used to perform unsupervised principal component analysis (PCA). VIP $\geq$ 1, p-value $<$ 0.05, and absolute Log2FC $\geq$ 1 were used to identify significantly regulated metabolites across groups. The Mann-Whitney U-test was used for each metabolite to compute the p-value for significance. VIP values were calculated using the R package MetaboAnalystR and retrieved from the OPLS-DA data, which included included score plots and permutation plots. The cor function in R was used to generate the Spearman correlation coefficient between samples,

which was then shown as heatmaps. The KEGG database (http://www.kegg.jp/kegg) was used to annotate the identified metabolites, and the annotated metabolites were then linked to the KEGG pathway database. A hypergeometric *p*-value test was used to find pathways that had significantly modulated metabolites.

GPR43 agonist treatment

For irradiated HIEC-6 cells co-cultured with *A. muciniphila* or treated with 3HB, vehicle [10% DMSO (D2650, Sigma-Aldrich) + 40% PEG300 (HY-Y0873, MCE) + 5% Tween 80 (HY-Y1891, MCE) + 45% saline] was used to resuspend bacteria or dissolve 3HB. Irradiated cells were treated with 10 μM GPR43 agonist (4-CMTB,[51] HY-P1125, MCE) or vehicle and then the expression of IL6 was assessed. To determine the effect of the GPR43 agonist on mice, RP mice pretreated with antibiotics were orally gavaged with 200 μL 3HB (150 mg/kg body weight) or saline and were injected with 200 μL 4CMTB (10 mg/kg body weight) or vehicle. Clinical score plots and samples were obtained following five weeks of treatment.

Data analysis

GraphPad Prism 6 (GraphPad Software, USA) was used for statistical analysis. The figure legends indicated the number of animals (n) used in the studies. One dot or lane indicated one mouse or sample. All values were shown as the mean ± SEM, with $*P < 0.05$, $**P < 0.01$, $***P < 0.001$, $****P < 0.0001$; ns, not significant. The D'Agostino-Pearson omnibus test was used to determine data normal distributions. If statistical significance between two groups was not mentioned in the figure legends, it was calculated using an unpaired, two-tailed Student's *t* test, Mann-Whitney test, or permutation multivariate analysis of variance (PERMANOVA) test, and significance of more than two groups was established using one-way ANOVA or two-way ANOVA in GraphPad Prism with the default setting depending on experience.

Data Availability: Data of 16S rDNA sequencing are available in a public repository at https://dataview.ncbi.nlm.nih.gov/. The accession numbers of 16S rDNA sequencing data are PRJNA881491 and PRJNA881495. All other data supporting the findings of this study are available from the corresponding authors on reasonable request.

Supplemental Data: This article contains supplemental data.

Conflict of Interest: The authors declare no competing interests.

Acknowledgments: This work was supported by the Guangdong key areas R & D projects (2018B020205002 to YJL), Guang Dong Cheung Kong Philanthropy Foundation (E2018096 to YJL), Guangzhou key R & D project (202206080008 to YJL), National Natural Science Foundation of China (82103084 to HM.W), and Sun Yat-sen University Clinical Research 5010 Program (2019021 to HM.W).

Author Contributions: ZG, HM.W, HW, YL planned the experiments. ZG, CC, JC, ZJ, LC, YW, HC performed the experiments and analysis. ZG, YL wrote the draft of the manuscript. All authors contributed to the edits of the manuscript.

Reference

1. Lam SY, Peppelenbosch MP, Fuhler GM. Prediction and Treatment of Radiation Enteropathy: Can Intestinal Bugs Lead the Way? Clin Cancer Res 2019;25:6280-6282.
2. Hauer-Jensen M, Denham JW, Andreyev HJ. Radiation enteropathy--pathogenesis, treatment and prevention. Nat Rev Gastroenterol Hepatol 2014;11:470-9.
3. Reis Ferreira M, Andreyev HJN, Mohammed K, et al. Microbiota- and Radiotherapy-Induced Gastrointestinal Side-Effects (MARS) Study: A Large Pilot Study of the Microbiome in Acute and Late-Radiation Enteropathy. Clin Cancer Res 2019;25:6487-6500.
4. Shadad AK, Sullivan FJ, Martin JD, et al. Gastrointestinal radiation injury: prevention and treatment. World J Gastroenterol 2013;19:199-208.
5. Lenz L, Rohr R, Nakao F, et al. Chronic radiation proctopathy: A practical review of endoscopic treatment. World J Gastrointest Surg 2016;8:151-60.
6. Wu P, Li L, Wang H, et al. Role of Angiogenesis in Chronic Radiation Proctitis: New Evidence Favoring Inhibition of Angiogenesis Ex Vivo. Dig Dis Sci 2018;63:113-125.
7. Indaram AV, Visvalingam V, Locke M, et al. Mucosal cytokine production in radiation-induced proctosigmoiditis compared with inflammatory bowel disease. Am J Gastroenterol 2000;95:1221-5.
8. Ferreira MR, Muls A, Dearnaley DP, et al. Microbiota and radiation-induced bowel toxicity: lessons from inflammatory bowel disease for the radiation oncologist. Lancet Oncol 2014;15:e139-47.

9. Kumagai T, Rahman F, Smith AM. The Microbiome and Radiation Induced-Bowel Injury: Evidence for Potential Mechanistic Role in Disease Pathogenesis. Nutrients 2018;10.
10. Gerassy-Vainberg S, Blatt A, Danin-Poleg Y, et al. Radiation induces proinflammatory dysbiosis: transmission of inflammatory susceptibility by host cytokine induction. Gut 2018;67:97-107.
11. Guo H, Chou WC, Lai Y, et al. Multi-omics analyses of radiation survivors identify radioprotective microbes and metabolites. Science 2020;370.
12. Symon Z, Goldshmidt Y, Picard O, et al. A murine model for the study of molecular pathogenesis of radiation proctitis. Int J Radiat Oncol Biol Phys 2010;76:242-50.
13. Schirmer M, Franzosa EA, Lloyd-Price J, et al. Dynamics of metatranscription in the inflammatory bowel disease gut microbiome. Nat Microbiol 2018;3:337-346.
14. Fujimura KE, Lynch SV. Microbiota in allergy and asthma and the emerging relationship with the gut microbiome. Cell Host Microbe 2015;17:592-602.
15. Fischbach MA, Segre JA. Signaling in Host-Associated Microbial Communities. Cell 2016;164:1288-1300.
16. Cani PD. Microbiota and metabolites in metabolic diseases. Nat Rev Endocrinol 2019;15:69-70.
17. Fan Y, Pedersen O. Gut microbiota in human metabolic health and disease. Nat Rev Microbiol 2021;19:55-71.
18. Skelly AN, Sato Y, Kearney S, et al. Mining the microbiota for microbial and metabolite-based immunotherapies. Nat Rev Immunol 2019;19:305-323.

19. Lu W, Xie Y, Huang B, et al. Platelet-derived growth factor C signaling is a potential therapeutic target for radiation proctopathy. Sci Transl Med 2021;13.
20. Grodsky MB, Sidani SM. Radiation proctopathy. Clin Colon Rectal Surg 2015;28:103-11.
21. Koh WJ, Abu-Rustum NR, Bean S, et al. Cervical Cancer, Version 3.2019, NCCN Clinical Practice Guidelines in Oncology. J Natl Compr Canc Netw 2019;17:64-84.
22. Hotamisligil GS. Inflammation, metaflammation and immunometabolic disorders. Nature 2017;542:177-185.
23. Puchalska P, Crawford PA. Multi-dimensional Roles of Ketone Bodies in Fuel Metabolism, Signaling, and Therapeutics. Cell Metab 2017;25:262-284.
24. Tan JK, McKenzie C, Marino E, et al. Metabolite-Sensing G Protein-Coupled Receptors-Facilitators of Diet-Related Immune Regulation. Annu Rev Immunol 2017;35:371-402.
25. Tanaka T, Narazaki M, Kishimoto T. IL-6 in inflammation, immunity, and disease. Cold Spring Harb Perspect Biol 2014;6:a016295.
26. Mierziak J, Burgberger M, Wojtasik W. 3-Hydroxybutyrate as a Metabolite and a Signal Molecule Regulating Processes of Living Organisms. Biomolecules 2021;11.
27. Zhang H, Liu Y, Yao C, et al. FabG can function as PhaB for poly-3-hydroxybutyrate biosynthesis in photosynthetic cyanobacteria Synechocystis sp. PCC 6803. Bioengineered 2017;8:707-715.
28. Zhang YM, Rock CO. Evaluation of epigallocatechin gallate and related plant polyphenols as inhibitors of the FabG and FabI reductases of bacterial type II fatty-acid synthase. J Biol Chem 2004;279:30994-1001.

29. Andreyev HJ. GI Consequences of Cancer Treatment: A Clinical Perspective. Radiat Res 2016;185:341-8.
30. Andreyev J. Gastrointestinal complications of pelvic radiotherapy: are they of any importance? Gut 2005;54:1051-4.
31. Li Z, Zhang S, Zhang Y, et al. Applications and Mechanism of 3-Hydroxybutyrate (3HB) for Prevention of Colonic Inflammation and Carcinogenesis as a Food Supplement. Mol Nutr Food Res 2021;65:e2100533.
32. Dmitrieva-Posocco O, Wong AC, Lundgren P, et al. beta-Hydroxybutyrate suppresses colorectal cancer. Nature 2022;605:160-165.
33. Hirata Y, Shimazaki S, Suzuki S, et al. beta-hydroxybutyrate suppresses NLRP3 inflammasome-mediated placental inflammation and lipopolysaccharide-induced fetal absorption. J Reprod Immunol 2021;148:103433.
34. Youm YH, Nguyen KY, Grant RW, et al. The ketone metabolite beta-hydroxybutyrate blocks NLRP3 inflammasome-mediated inflammatory disease. Nat Med 2015;21:263-9.
35. Chen L, Zhang G, Li G, et al. Ifnar gene variants influence gut microbial production of palmitoleic acid and host immune responses to tuberculosis. Nat Metab 2022;4:359-373.
36. Rao Y, Kuang Z, Li C, et al. Gut Akkermansia muciniphila ameliorates metabolic dysfunction-associated fatty liver disease by regulating the metabolism of L-aspartate via gut-liver axis. Gut Microbes 2021;13:1-19.
37. Cani PD, Depommier C, Derrien M, et al. Akkermansia muciniphila: paradigm for next-generation beneficial microorganisms. Nat Rev Gastroenterol Hepatol 2022.

38. Masui R, Sasaki M, Funaki Y, et al. G protein-coupled receptor 43 moderates gut inflammation through cytokine regulation from mononuclear cells. Inflamm Bowel Dis 2013;19:2848-56.

39. Maslowski KM, Vieira AT, Ng A, et al. Regulation of inflammatory responses by gut microbiota and chemoattractant receptor GPR43. Nature 2009;461:1282-6.

40. Sina C, Gavrilova O, Forster M, et al. G protein-coupled receptor 43 is essential for neutrophil recruitment during intestinal inflammation. J Immunol 2009;183:7514-22.

41. Kim MH, Kang SG, Park JH, et al. Short-chain fatty acids activate GPR41 and GPR43 on intestinal epithelial cells to promote inflammatory responses in mice. Gastroenterology 2013;145:396-406 e1-10.

42. Smith PM, Howitt MR, Panikov N, et al. The microbial metabolites, short-chain fatty acids, regulate colonic Treg cell homeostasis. Science 2013;341:569-73.

43. Vieira AT, Macia L, Galvao I, et al. A Role for Gut Microbiota and the Metabolite-Sensing Receptor GPR43 in a Murine Model of Gout. Arthritis Rheumatol 2015;67:1646-56.

44. Kimura I, Ichimura A, Ohue-Kitano R, et al. Free Fatty Acid Receptors in Health and Disease. Physiol Rev 2020;100:171-210.

45. Xu F, Su C, Wu T, et al. [CRISPR/Cas9-based knockout of GPR43 gene in RAW264.7 cells inhibits their phagocytosis to Klebsiella pneumoniae]. Xi Bao Yu Fen Zi Mian Yi Xue Za Zhi 2020;36:481-486.

46. Nadeem A, Ahmad SF, Al-Harbi NO, et al. GPR43 activation enhances psoriasis-like inflammation through epidermal upregulation of IL-6 and dual oxidase 2 signaling in a murine model. Cell Signal 2017;33:59-68.
47. Abraham C, Cho JH. Inflammatory bowel disease. N Engl J Med 2009;361:2066-78.
48. Delia P, Sansotta G, Donato V, et al. Use of probiotics for prevention of radiation-induced diarrhea. World J Gastroenterol 2007;13:912-5.
49. Chitapanarux I, Chitapanarux T, Traisathit P, et al. Randomized controlled trial of live lactobacillus acidophilus plus bifidobacterium bifidum in prophylaxis of diarrhea during radiotherapy in cervical cancer patients. Radiat Oncol 2010;5:31.
50. Langberg CW, Waldron JA, Baker ML, et al. Significance of overall treatment time for the development of radiation-induced intestinal complications. An experimental study in the rat. Cancer 1994;73:2663-8.
51. Grundmann M, Tikhonova IG, Hudson BD, et al. A Molecular Mechanism for Sequential Activation of a G Protein-Coupled Receptor. Cell Chem Biol 2016;23:392-403.

Figure and figure legends

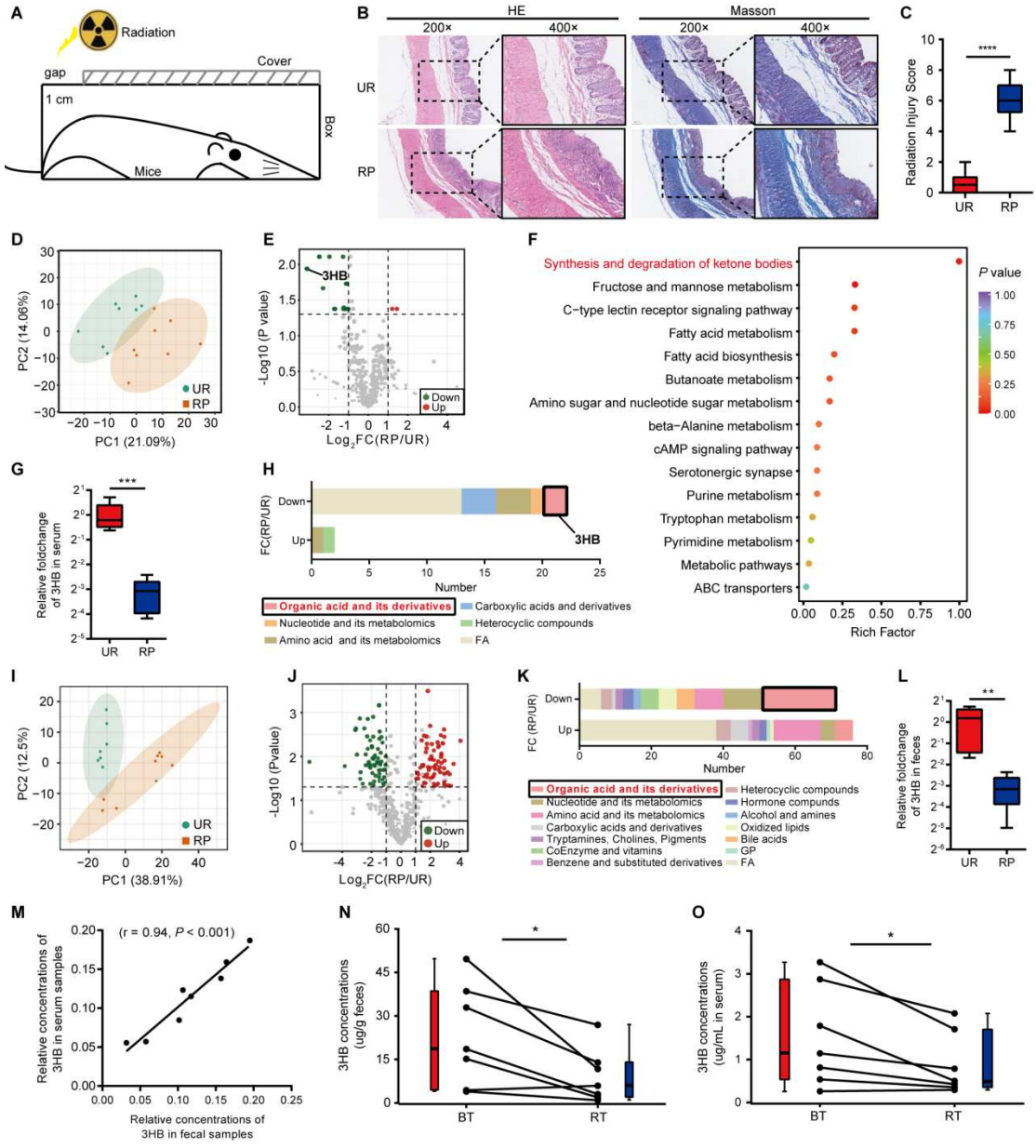

Figure 1. Gut co-metabolite 3HB is downregulated in RP mice and patients.

(A) Experimental design schematic of localized internal rectal radiation in C57BL/6J mice.

(**B**) Representative images of H&E and Masson immunostaining of the distal rectums. Insets are demonstrated in higher magnification on the right.

(**C**) Histopathological change evaluated by calculating the radiation injury score (RIS).

(**D**) PCA plot of serum metabolites from UR and RP mice.

(**E**) Volcano plot of all metabolites found in serum samples. Red points indicate metabolites with a VIP (variable importance in projection) score > 1 and an adjusted $P < 0.05$ and log2(RP/UR) > 1; green points indicate metabolites with a VIP score > 1 and an adjusted $P < 0.05$ and log2(RP/UR) < -1.

(**F**) KEGG pathway enrichment analysis of differentially enriched metabolites in serum between RP and UR mice.

(**G**) Relative abundance of 3HB in serum between RP and UR mice.

(**H**) Cluster analysis of differentially enriched metabolites in serum between RP and UR mice.

(**I**) PCA plot of fecal metabolites from UR and RP mice.

(**J**) Volcano plot of all metabolites found in fecal samples. Red points indicate metabolites with a VIP (variable importance in projection) score > 1 and an adjusted $P < 0.05$ and log2(RP/UR) > 1; green points indicate metabolites with a VIP score > 1 and an adjusted $P < 0.05$ and log2(RP/UR) < -1.

(**K**) Cluster analysis of differentially enriched metabolites in fecal samples between RP and UR mice.

(**L**) Relative abundance of 3HB in fecal samples between RP and UR mice.

(**M**) Correlation of 3HB between serum and fecal samples measured in RP mice.

(**N-O**) Detection of 3HB concentrations in fecal (N) and serum (O) samples derived from oncology patients before (BT) and after (RT) radiotherapy treatment.

Data are presented as the mean ± SEM. N = 8 per group in mouse model. N = 7 for oncology patients. Histological analysis of the rectal tissue was performed 8 weeks after irradiation. $*P < 0.05$, $**P < 0.01$, $***P < 0.001$, and $****P < 0.0001$ determined by the Student's *t*-test [(C), (H), and (L)], Spearman correlation (M) and paired exact Wilcoxon test, two tailed [(N), and (O)].

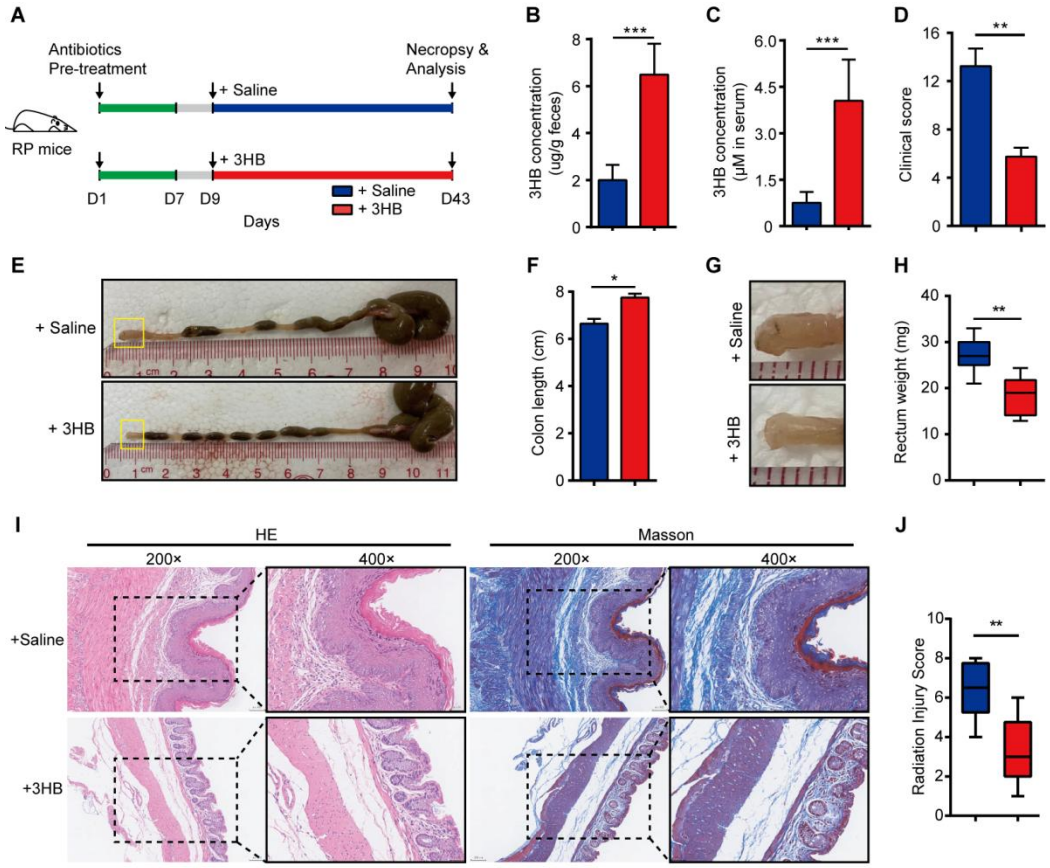

Figure 2. Oral administration of 3HB ameliorates radiation-induced damage.

(**A**) Experimental diagram for determining the role of 3HB in RP mice. RP mice pretreated with antibiotics for one week were orally administered with 3HB (150 mg/kg body weight) or saline 3 times per week.

(**B-C**) Concentrations of 3HB in fecal (B) and serum (C) samples.

(**D**) Clinical scores of the mice in each group.

(**E-F**) Representative images of the colon (E) and colon length statistics (F). Boxed regions are showed at a higher magnification in G.

(**G-H**) Representative images of the rectum (G) and rectum weight statistics (H).

(**I**) Representative images of H&E and Masson immunostaining of the distal rectum. Insets are showed at a higher magnification on the right.

(**J**) Histopathological changes evaluated by calculating the radiation injury scores (RIS).

Data are presented as the mean ± SEM. N = 8 per group. Histological analysis of the samples was performed 5 weeks after treatment. *P < 0.05, **P < 0.01 and ***P < 0.001 determined by the Student's t-test [(B), (C), (D), (E), (G), (I), (K), (L), and (M)].

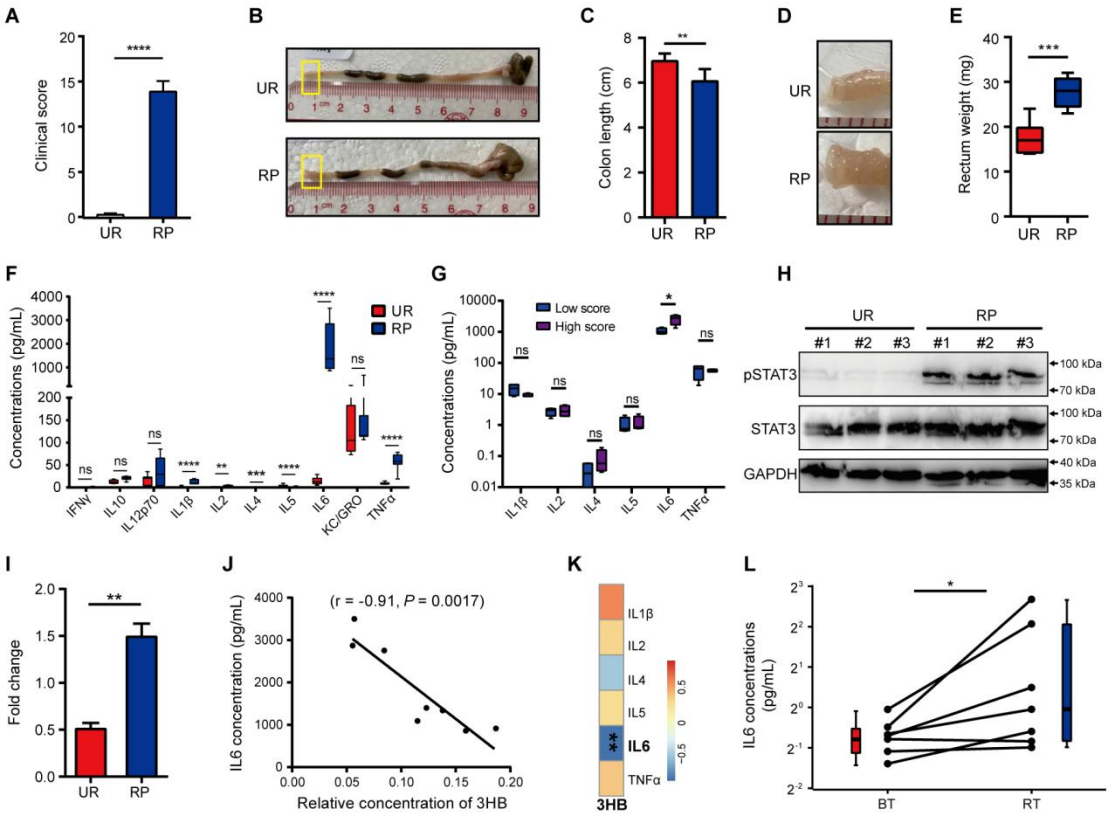

Figure 3. The concentration of 3HB is negatively associated with the expression of proinflammatory IL6 that increased along with the severity of radiation damage.

(**A**) Clinical score of RP and UR mice 8 weeks after exposure to or without 25 Gy irradiation.

(**B-C**) Representative images of the colon (B) and colon length statistics (C). Boxed regions shown at higher magnification in D.

(**D-E**) Representative images of the rectum (D) and rectum weight statistics (E).

(**F**) Pooled bar graph data show the expression levels of IFNγ, IL10, IL12p70, IL1β, IL2, IL4, IL5, IL6, KC/GRO, and TNFα in the animal sera.

(**G**) The 6 differential cytokines involved in the disease severity in RP mice.

(**H**) Western blot for phosphorylated and total STAT3 in rectal tissue. Glyceraldehyde-3-phosphate dehydrogenase (GAPDH) served as a loading control.

(**I**) Quantitative immunoblot analysis of pSTAT3 expression (compared to STAT3 and GAPDH) calculated by ImageJ.

(**J**) Correlation between 3HB concentration and IL6 expression in sera of RP mice.

(**K**) Heatmap showing correlations between 6 differential cytokines and 3HB in RP mice.

(**L**) Detection of IL6 expression in serum samples derived from oncology patients before (BT) and after (RT) radiotherapy treatment.

Data are presented as the mean ± SEM. N = 8 per group in mouse model. N = 7 for oncology patients. Histological analysis of the rectal tissue was performed 8 weeks after irradiation. $*P < 0.05$, $**P < 0.01$, $***P < 0.001$, and $***P < 0.0001$ determined by the Student's *t*-test [(C), (E), (F), (G), and (I)], Mann–Whitney U test (A), Spearman correlation [(J), and (K)] and paired exact Wilcoxon test, two tailed (L).

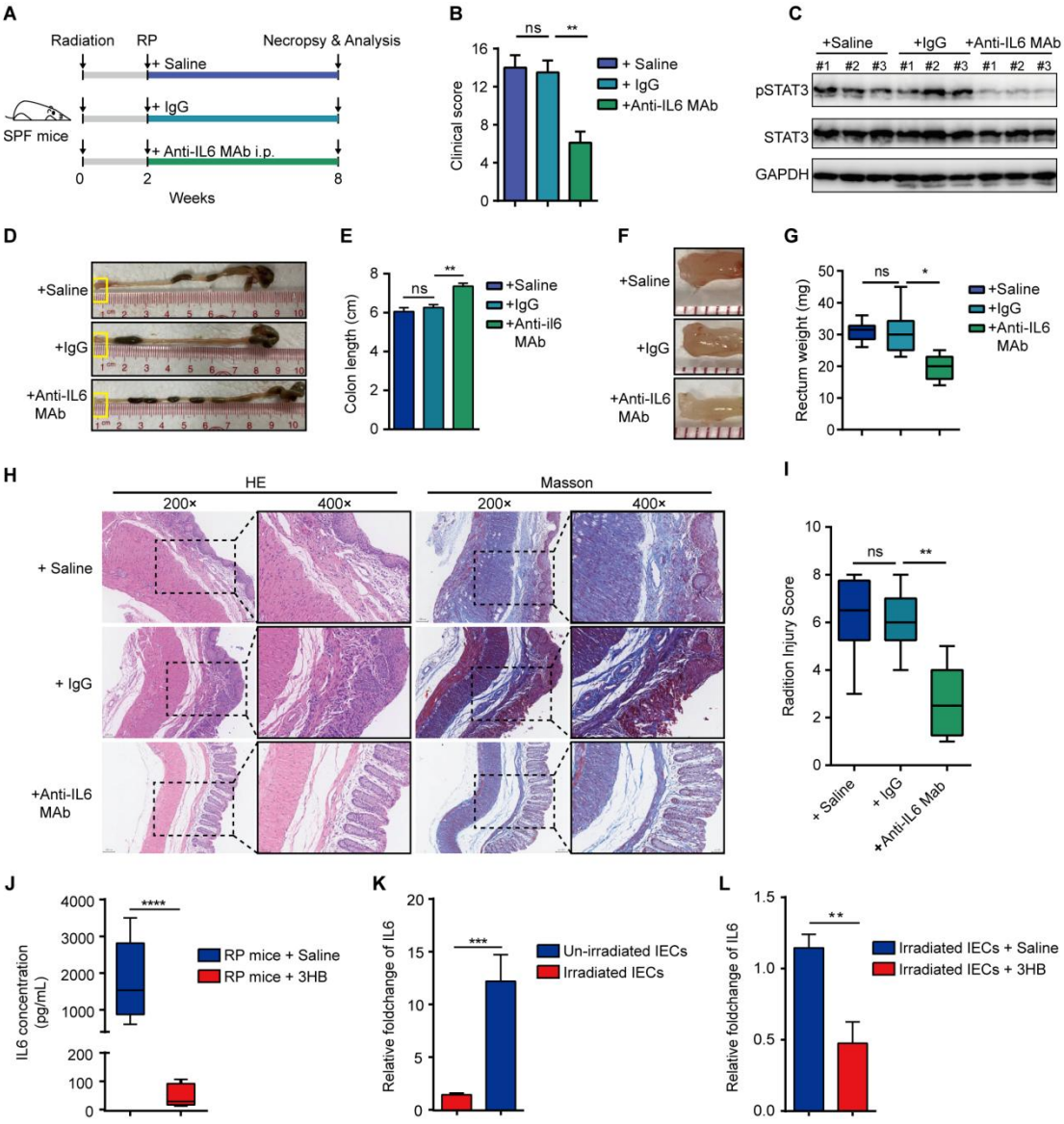

Figure 4. 3HB can downregulate the radiation-induced expression of IL6, a key mediator involved in RP damage.

(**A**) Experimental diagram for determining whether the blockage of IL6 signaling has protective effect in the RP mice. Mice were injected with 5 mg/kg anti-IL6 MAb or IgG antibody control or vehicle and injections were given every two days for 6 weeks.

(**B**) Clinical score for the mice in each group.

(**C**) Western blot for phosphorylated and total STAT3 in rectal tissue. GAPDH served as a loading control.

(**D-E**) Representative images of the colon (D) and colon length statistics (E). Boxed regions shown at higher magnification in F.

(**F-G**) Representative images of the rectum (F) and rectum weight statistics (G).

(**H**) Representative images of H&E and Masson immunostaining of the distal rectums. Insets are demonstrated in higher magnification at right.

(**I**) Histopathological change evaluated by calculating the radiation injury score (RIS).

(**J**) Expression level of IL6 in the animal sera of RP mice treated with 3HB or Saline.

(**K**) Expression level of IL6 in irradiated or unirradiated HIEC-6 epithelial cells (IECs).

(**L**) Expression level of IL6 in irradiated HIEC-6 epithelial cells (IECs) treated with 3HB (10 mM) or saline.

Data are presented as the mean ± SEM. N = 8 for saline and anti-IL6 MAb treated groups; N = 7 for IgG treated group. Histological analysis of the rectal tissue was performed 6 weeks post-injection. $*P < 0.05$, $**P < 0.01$, $***P < 0.001$, and $****P < 0.001$ determined by the one-way ANOVA with Tukey's multiple comparison test [(B), (E), (G), and (I)] and Student's *t*-test [(J), (K), and (L)].

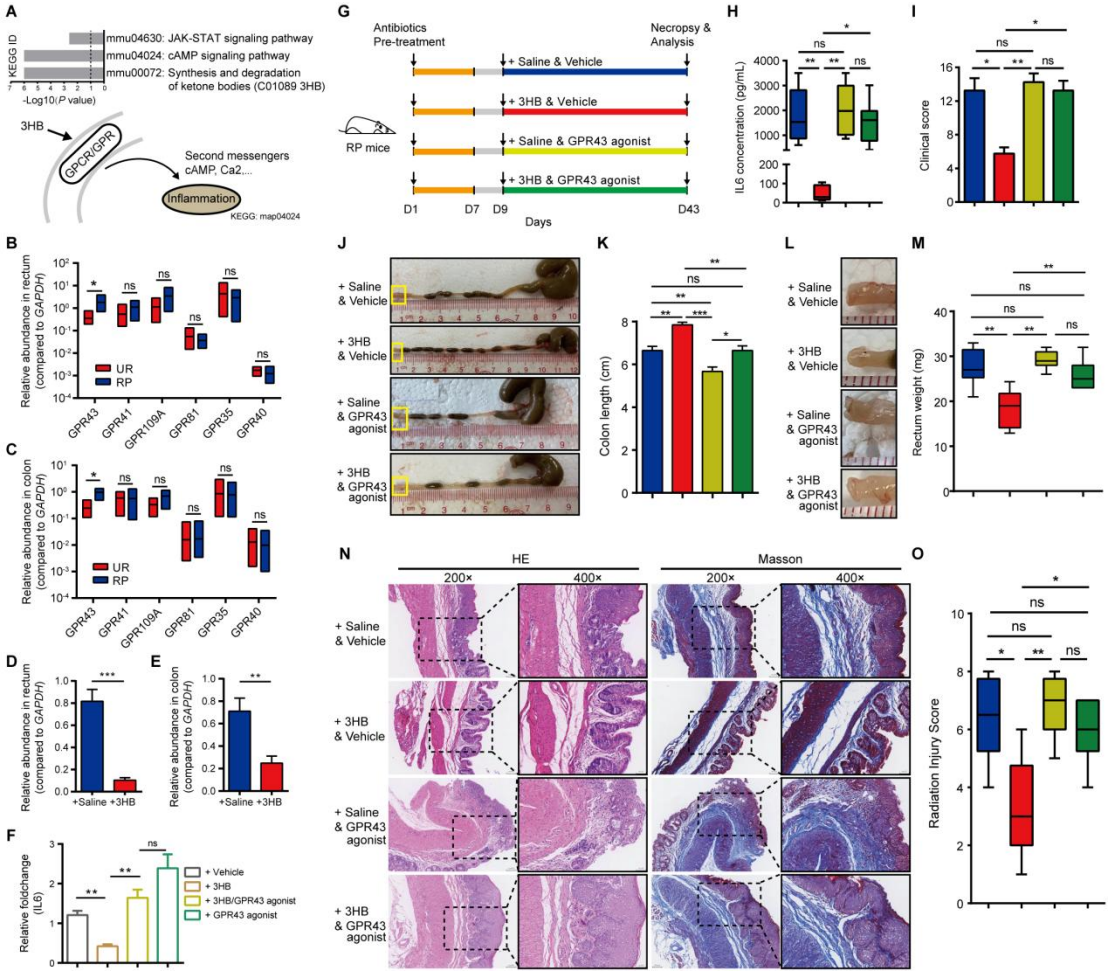

Figure 5. The radioprotective effect of 3HB is mediated by GPR43.

(**A**) Metabolic network integrated biochemical pathways and chemical relationships of 3HB derived from RP and UR mice.

(**B-C**) The expression of GPR receptors (GPR43, GPR41, GPR109A, GPR81, GPR35, and GPR40) was assessed by quantitative PCR using mRNA extracted from the rectal (B) and colon samples (C) derived from UR and RP mice. Results for UR and RP mice are in red and blue, respectively.

(**D-E**) Expression of GPR43 was assessed by qPCR-based analysis using mRNA extracted from the rectal (D) and colon samples (E). Results for RP mice treated with 3HB or saline are showed in red and blue, respectively.

(**F**) The expression level of IL6 in irradiated IECs treated with vehicle (+ Vehicle), 3HB (+ 3HB), 3HB and GPR43 agonist (+ 3HB/GPR43 agonist), and GPR43 agonist (+ GPR43 agonist). GPR43 agonist (4CMTB, 10 μM), 3HB (10 mM), and vehicle (10% DMSO, 40% PEG300, 5% Tween 80, 45% saline).

(**G**) Experimental diagram for determining whether the activation of GPR43 blocks the protective effect in the RP mice. Mice pre-treated with antibiotics were orally administrated with 3HB (150 mg/kg body weight) or saline 3 times per week. Mice were injected with GPR43-synthetic agonist (4CMTB, 10 mg/kg body weight) or vehicle (10% DMSO + 40% PEG300 + 5% Tween 80 + 45% saline) 3 times per week at the same time.

(**H**) Concentration of IL6 in the animal sera.

(**I**) Clinical score of the mice in each group.

(**J-K**) Representative images of the colon (J) and colon length statistics (K). Boxed regions are showed at higher magnification in L.

(**L-M**) Representative images of the rectum (L) and rectum weight statistics (M).

(**N**) Representative images of H&E and Masson immunostaining of the distal rectums. Insets are demonstrated in higher magnification at right.

(**O**) Histopathological change evaluated by calculating the radiation injury score (RIS). Data are presented as the mean ± SEM. N = 8 for the vehicle injected group; N = 7 for the GPR43 agonist injected group. Histological analysis of the rectal tissue was performed 5 weeks after administration and injection. $*P < 0.05$, $**P < 0.01$, and $***P < 0.001$ determined by the Student's *t*-test [(B), (C), (D), and (E)], one-way ANOVA with Tukey's multiple comparison test [(F), (H), (I), (K), (M), and (O)].

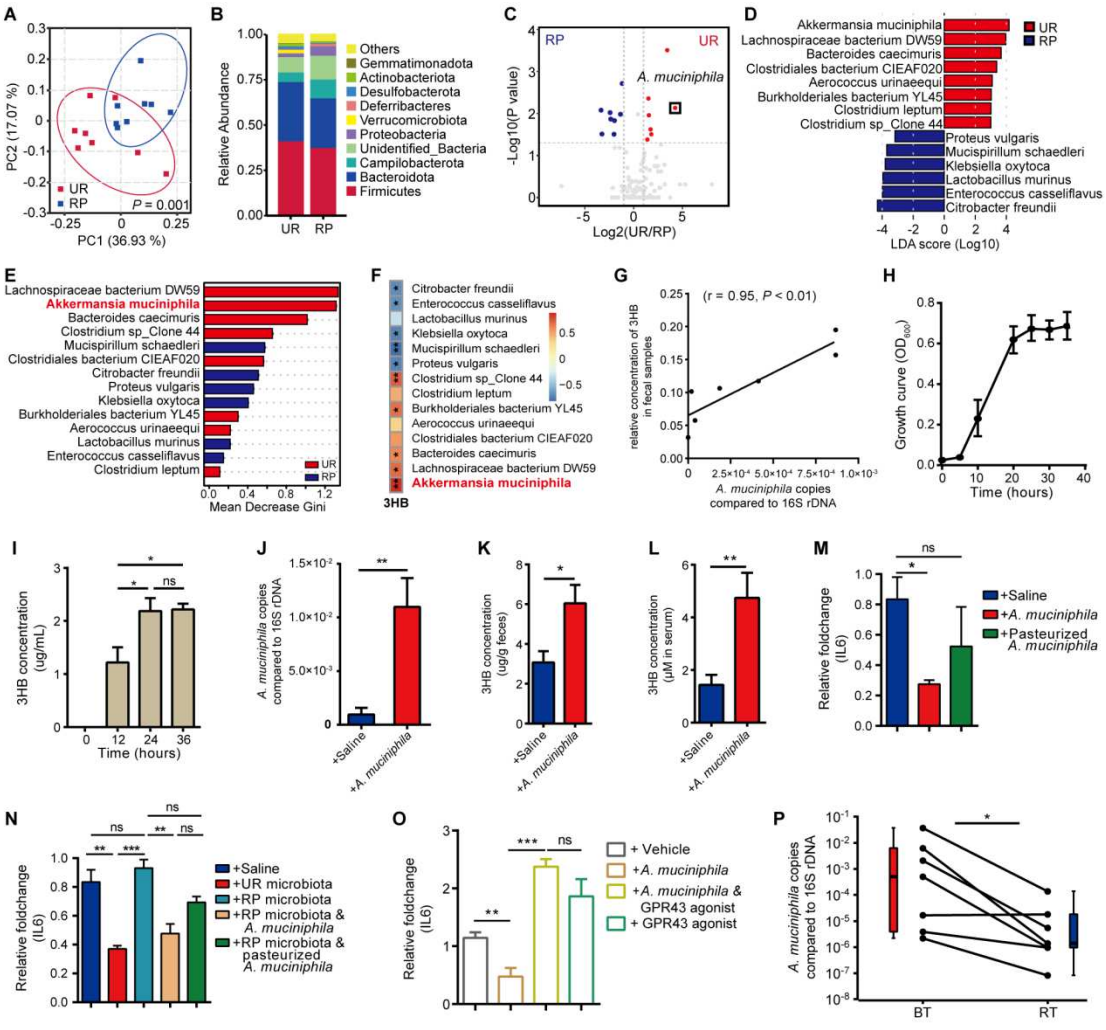

Figure 6. The significant reduced *A. muciniphila* in radiation-reshaped gut bacteria is positively associated with lower 3HB concentration, can produce 3HB and downregulate IL6 expression *via* GPR43.

(**A**) Principal co-ordinates analysis (PCoA) plot (based on weighted UniFrac distances).

(**B**) The relative abundance of gut bacteria at phylum level in the fecal samples.

(**C**) Volcano plot of all bacterial species found in fecal samples. Red points indicate species with an adjusted $P < 0.05$ and $\log2(UR/RP) > 1$; green points indicate species with an adjusted $P < 0.05$ and $\log2(UR/RP) < -1$. *A. muciniphila* (black box) is a more abundant species enriched in UR (i.e., significantly reduced in RP mice).

(**D**) Histogram of the linear discriminant analysis (LDA) coupled with effect size measurements (LEfSe) [LDA significant threshold (log10) > ±3] identified taxonomic biomarkers at species level between UR and RP. Higher abundant species in UR and RP are shaded in red and blue, respectively.

(**E**) Predictive importance of selected species enriched by LEfSe analysis was assessed by random forest analysis.

(**F**) Heatmap showing correlations between 3HB concentration and the abundance of LEfSe-enriched species in RP mice.

(**G**) Correlation between 3HB concentration and *A. muciniphila* abundance in fecal samples of RP mice.

(**H**) Growth curve of *A. muciniphila* cultured in BHI under anaerobic conditions.

(**I**) Measurement of 3HB concentration in cultured *A. muciniphila* supernatant at the indicated time points.

(**J**) Analysis of *A. muciniphila* abundance in stool samples from RP mice with gavage of *A. muciniphila*.

(**K-L**) Gavage of *A. muciniphila* increased the concentration of 3HB in fecal (K) and serum (L) samples from RP mice.

(**M**) IL6 expression in irradiated IECs treated with *A. muciniphila*, inactivated *A. muciniphila* and saline, respectively.

(**N**) IL6 expression in irradiated IECs co-cultured with fecal bacterial suspensions obtained from RP mice 8 weeks post-radiation or from age-matched UR mice. Viable or non-viable *A. muciniphila* was added in the indicated group.

(**O**) IL6 expression level in irradiated IECs treated with vehicle (+ Vehicle), *A. muciniphila* (+ *A. muciniphila*), *A. muciniphila* and GPR43 agonist (+ *A. muciniphila*/GPR43 agonist), and GPR43 agonist (+ GPR43 agonist, 10 μM).

(**P**) Detection of *A. muciniphila* abundance in fecal samples derived from oncology patients before (BT) and after (RT) radiotherapy treatment.

Data are presented as the mean ± SEM. **P* < 0.05, ***P* < 0.01, and ****P* < 0.001 determined by the Student's *t*-test [(I), (J), (K), (L), and (M)], permutation multivariate analysis of variance (PERMANOVA) test (A), one-way ANOVA with Tukey's multiple comparison test [(N) and (O)], Spearman correlation [(F), and (G)] and paired exact Wilcoxon test, two tailed (P).

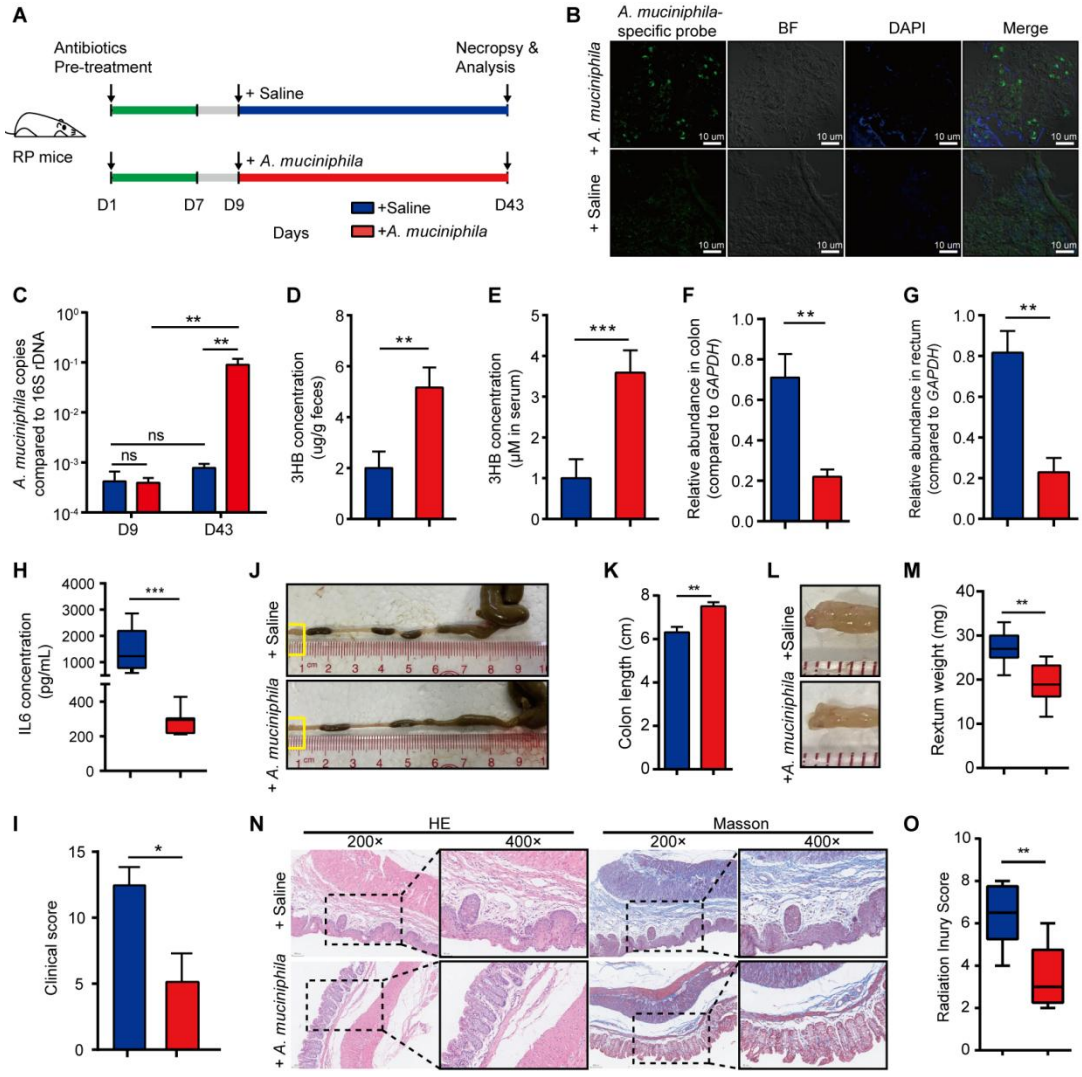

Figure 7. Gavage of *A. muciniphila* increases 3HB concentration, reduces IL6 expression and ameliorates radiation-induced damage in RP mice.

(**A**) Experimental diagram for determining the role of *A. muciniphila* in RP mice. RP mice pretreated with antibiotics for one week were orally administrated with *A. muciniphila* (2×10^8) or saline 3 times per week. Results for RP mice treated with *A. muciniphila* or saline are showed in red and blue, respectively.

(**B**) Representative fluorescent *in situ* hybridization (FISH) and confocal microscopic imaging analysis of *A. muciniphila* (green) in the intestinal mucosa using an *A. muciniphila*-specific probe. DAPI (4′, 6-diamidino-2-phenylindole) was used for nuclear staining (blue). Scale bars, 10 μm.

(**C**) Analysis of *A. muciniphila* abundance in stool samples from mice at days 9 and 37 after antibiotic treatment.

(**D-E**) 3HB shows much higher concentrations in fecal (D) and serum (E) samples from mice with oral administration of *A. muciniphila* than that treated with saline.

(**F-G**) Expression of GPR43 was assessed by qPCR-based analysis using mRNA extracted from the colon (F) and rectal samples (G).

(**H**) The expression of IL6 level in the animal sera.

(**I**) Clinical score of the mice in each group.

(**J-K**) Representative images of the colon (J) and colon length statistics (K). Boxed regions shown at higher magnification in L.

(**L-M**) Representative images of the rectum (L) and rectum weight statistics (M).

(**N**) Representative images of H&E and Masson immunostaining of the distal rectums. Insets are demonstrated in higher magnification at right.

(**O**) Histopathological change evaluated by calculating the radiation injury score (RIS). Data are presented as the mean ± SEM. N = 8 for the saline treated group and N = 7 for the *A. muciniphila* treated group. Histological analysis of the rectal tissue was performed 5 weeks after oral administration. $*P < 0.05$, $**P < 0.01$ and $***P < 0.001$ determined by the Student's *t*-test [(D), (E), (F), (G), (H), (I), (K), (M), and (O)], two-way ANOVA with Tukey's multiple comparison test (C).

Supplementary figure and figure legends

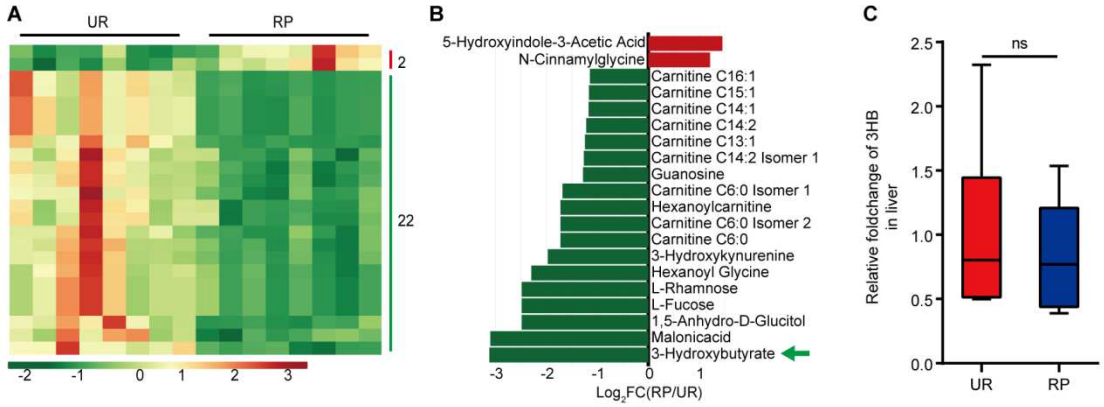

Figure S1. The concentrations of 3HB in serum that significantly decreased in RP mice are not related to liver.

(**A**) Heatmap of differentially enriched metabolites in serum samples between RP and UR mice.

(**B**) The top 20 significant differential metabolites in sera of RP and UR mice. Green arrowhead marks the 3HB.

(**C**) 3HB concentration shows no significant difference in liver after the treatment with radiation. ns, no significance, which is determined by the Student's *t*-test (C).

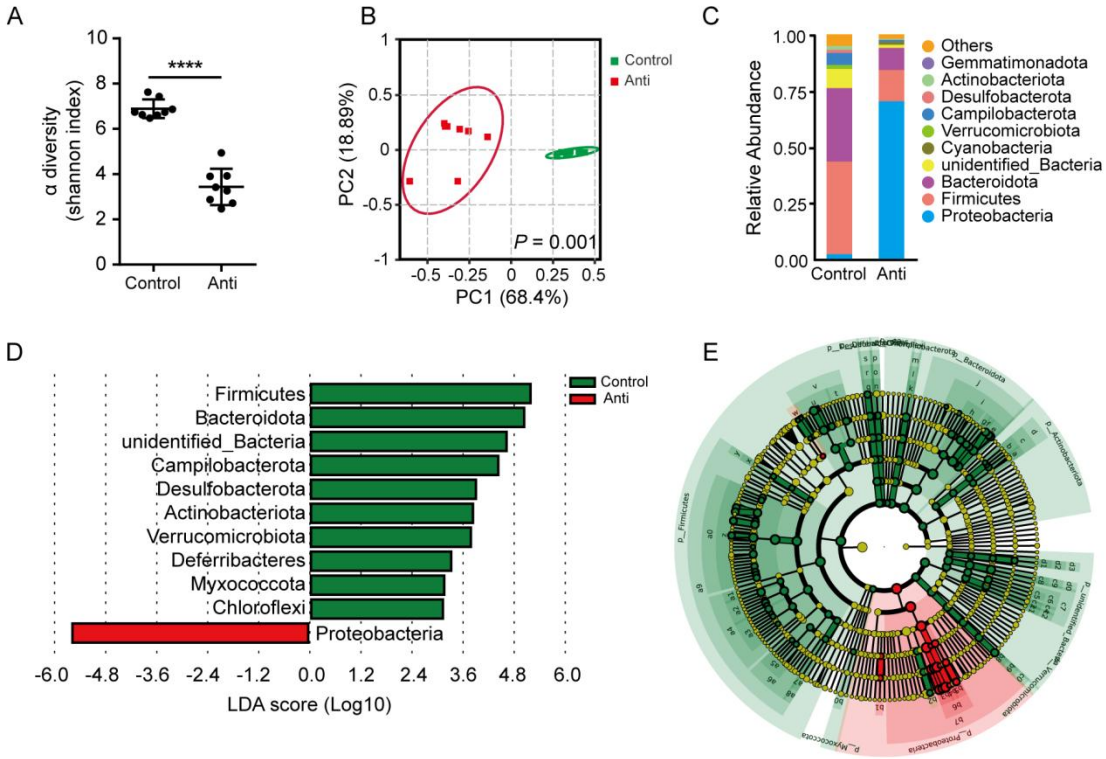

1240

1241 **Figure S2. Antibiotic treatment removes most of the bacteria from the intestine.**

1242 (**A**) Alpha (α) diversity with Shannon index is significant reduced in mice with the

1243 treatment of antibiotics compared to control mice.

1244 (**B**) Principal co-ordinates analysis (PCoA) plot (based on weighted UniFrac

1245 distances). *P* value is determined by the permutation multivariate analysis of variance

1246 (PERMANOVA) test.

1247 (**C**) The relative abundance of gut bacteria at phylum level in the fecal samples.

1248 (**D-E**) Histogram of the linear discriminant analysis (LDA) coupled with effect size

1249 measurements (LEfSe) [LDA significant threshold (log10) > ±3] (D) and cladogram

1250 tree (E) identified taxonomic biomarkers at phylum level between control and

1251 antibiotics treated mice. Higher abundant species in control mice (Control) and mice

1252 treated with antibiotics (Anti) are shaded in green and red, respectively.

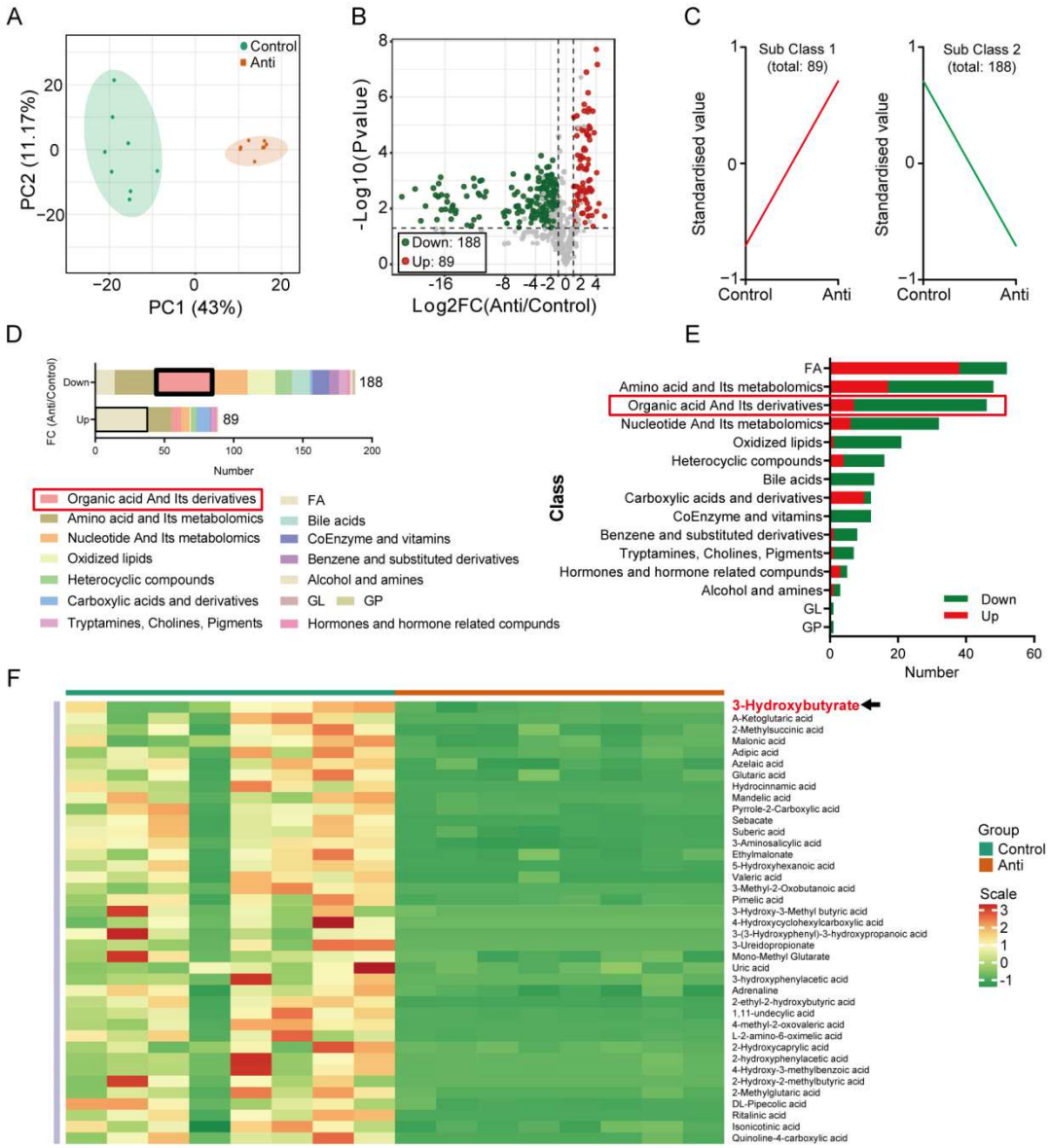

Figure S3. The concentration of many metabolites in feces is associated with antibiotic-removed gut bacteria, including organic acid and its derivatives with the most reduction in the absence of gut microbiota.

(**A**) PCA plot of feces metabolites from control mice (Control) and mice with antibiotics treatment (Anti).

(**B**) Volcano plot of all metabolites found in fecal samples. Red points indicate metabolites with a VIP (variable importance in projection) score > 1 and an adjusted $P < 0.05$ and log2(Anti/Control) > 1; green points indicate metabolites with a VIP score > 1 and an adjusted $P < 0.05$ and log2(Anti/Control) < -1.

(**C**) K-means analysis of the content change trend of metabolites in different samples.

(**D-E**) Cluster (D) and proportion (E) analysis of differentially enriched metabolites in feces between Control and Anti groups.

(**F**) Heatmap shows the significantly decreased metabolites in organic acids and their derivatives in fecal samples after antibiotic treatment.

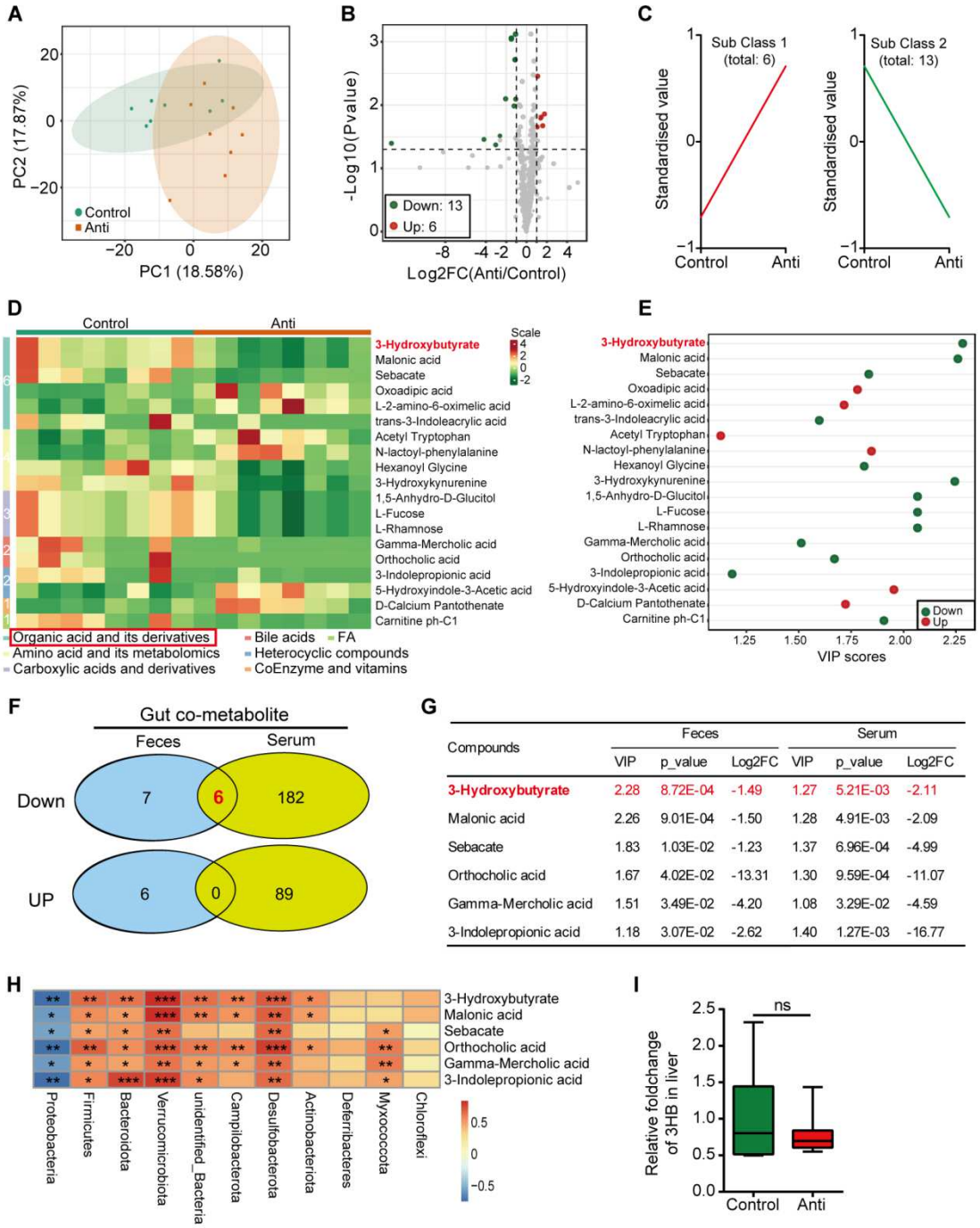

Compounds	Feces			Serum		
	VIP	p_value	Log2FC	VIP	p_value	Log2FC
3-Hydroxybutyrate	2.28	8.72E-04	-1.49	1.27	5.21E-03	-2.11
Malonic acid	2.26	9.01E-04	-1.50	1.28	4.91E-03	-2.09
Sebacate	1.83	1.03E-02	-1.23	1.37	6.96E-04	-4.99
Orthocholic acid	1.67	4.02E-02	-13.31	1.30	9.59E-04	-11.07
Gamma-Mercholic acid	1.51	3.49E-02	-4.20	1.08	3.29E-02	-4.59
3-Indolepropionic acid	1.18	3.07E-02	-2.62	1.40	1.27E-03	-16.77

Figure S4. The production of gut microbiota-derived 3HB in feces plays a dominant role in its concentration in serum.

(**A**) PCA plot of serum metabolites from control mice (Control) and mice with antibiotics treatment (Anti).

(**B**) Volcano plot of all metabolites found in serum samples. Red points indicate metabolites with a VIP (variable importance in projection) score > 1 and an adjusted

$P < 0.05$ and log2(Anti/Control) > 1; green points indicate metabolites with a VIP score > 1 and an adjusted $P < 0.05$ and log2(Anti/Control) < -1.

(**C**) K-means analysis of the content change trend of metabolites in different samples.

(**D**) Heatmap shows differentially enriched metabolites in sera between Control and Anti groups.

(**E**) VIP score of differential metabolites reveals their potential important role.

(**F-G**) Venn diagram (F) and list (G) display the six metabolites in sera that are directly associated with their feces concentration.

(**H**) Heatmap showing positive (red) and negative (blue) correlations between identified taxonomic biomarkers at phylum level (X axis) and fecal (Y axis) metabolites that are different in Control and Anti groups. $*P < 0.05$, $**P < 0.01$, and $***P < 0.001$ determined by the Spearman correlation.

(**I**) The ability of the liver to produce 3HB is not different in UR mice pre-treated with or without antibiotics. ns, no significance, which is determined by the Student's *t*-test.

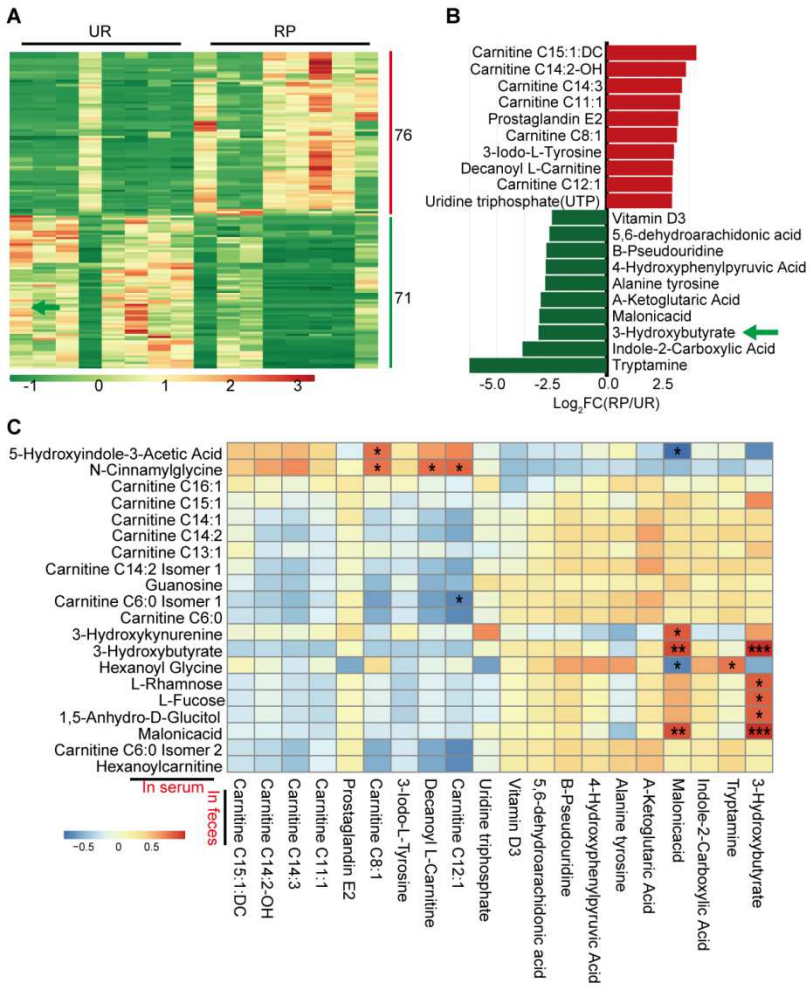

Figure S5. The concentrations of 3HB of stool and serum that significantly decreased in RP mice are positive correlation.

(**A**) Heatmap of enriched differential metabolites in fecal samples between RP and UR mice.

(**B**) The top 20 significant differential metabolites in feces of RP and UR mice. Green arrowhead marks the 3-hydroxybutyrate (3HB).

(**C**) Heatmap showing positive (red) and negative (blue) correlations between serum (X axis) and fecal (Y axis) metabolites measured in RP mice. **P* < 0.05, ***P* < 0.01, and ****P* < 0.001 determined by the Spearman correlation.

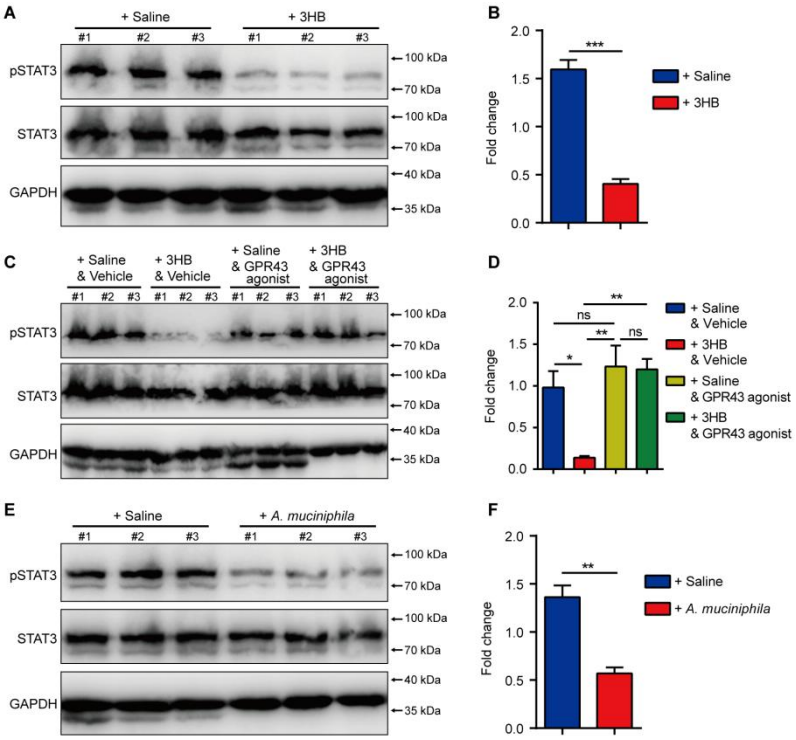

Figure S6. Western blot analysis of phosphorylated STAT3 in rectal tissue derived from RP mice with different treatments. Western blot for phosphorylated and total STAT3 in rectal tissue (left) and quantitative immunoblot analysis of pSTAT3 expression calculated by ImageJ (right). GAPDH served as a loading control. (**A-B**) RP mice pretreated with antibiotics for one week were orally administrated with 3HB (150 mg/kg body weight) or saline for 4 weeks (Figure 4).

(**C-D**) RP mice pretreated with antibiotics were orally administrated with 3HB (150 mg/kg body weight) or saline for 4 weeks. Mice were injected with GPR43 agonist (4CMTB, 10 mg/kg body weight) or vehicle (10% DMSO + 40% PEG300 + 5% Tween 80 + 45% saline) for 4 weeks at the same time (Figure 5).

(**E-F**) RP mice pretreated with antibiotics for one week were orally administrated with *A. muciniphila* (2×10^8) or saline for 4 weeks (Figure 7).

N = 3 biologically independent samples. Data are presented as the mean ± SEM. $*P < 0.05$, $**P < 0.01$, and $***P < 0.001$ determined by the Student's *t*-test [(B) and (F)] and one-way ANOVA with Tukey's multiple comparison test (D).

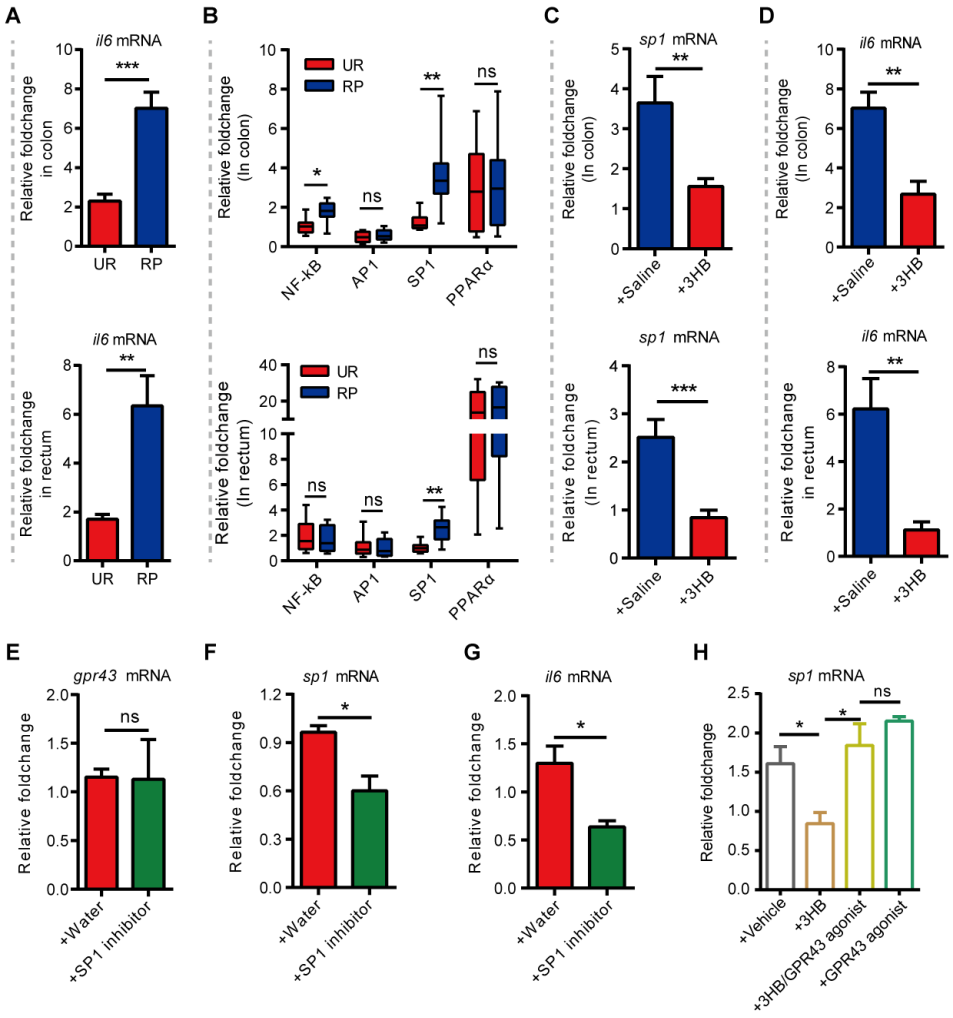

Figure S7. 3HB inhibits radiation-induced IL6 expression *via* transcriptional regulator SP1 mediated by GPR43.

(**A**) The expression of *il6* from the colon and rectal samples in the UR and RP mice.

(**B**) Detection of the expression of known IL6 transcriptional regulators (*NF-kB*, *AP1*, *SP1*, and *PPARα*) by quantitative PCR using mRNA extracted from the colon and rectal samples of UR and RP mice, respectively.

(**C**) The expression of *sp1* from the colon and rectal samples in the RP mice treated with 3HB or saline.

(**D**) The expression of *il6* from the colon and rectal samples in the RP mice treated with 3HB or saline.

(**E-G**) The expression of *gpr43*, *sp1*, and *il6* in irradiated IECs treated with SP1 inhibitor (mithramycin, 25 nM) (MCE, HY-A0122).

(**H**) The expression of *sp1* in irradiated IECs treated with vehicle (+ Vehicle), 3HB (+ 3HB), 3HB and GPR43 agonist (+ 3HB/GPR43 agonist), and GPR43 agonist (+ GPR43 agonist). GPR43 agonist (4CMTB, 10 μM), 3HB (3-hydroxybutyrate, 10 mM), and vehicle (10% DMSO, 40% PEG300, 5% Tween 80, 45% saline).

Data are presented as the mean ± SEM. $*P < 0.05$, $**P < 0.01$, and $***P < 0.001$ determined by the Student's *t*-test [(A), (B), (C), (D), (E), (F), and (G)] and one-way ANOVA with Tukey's multiple comparison test (H).

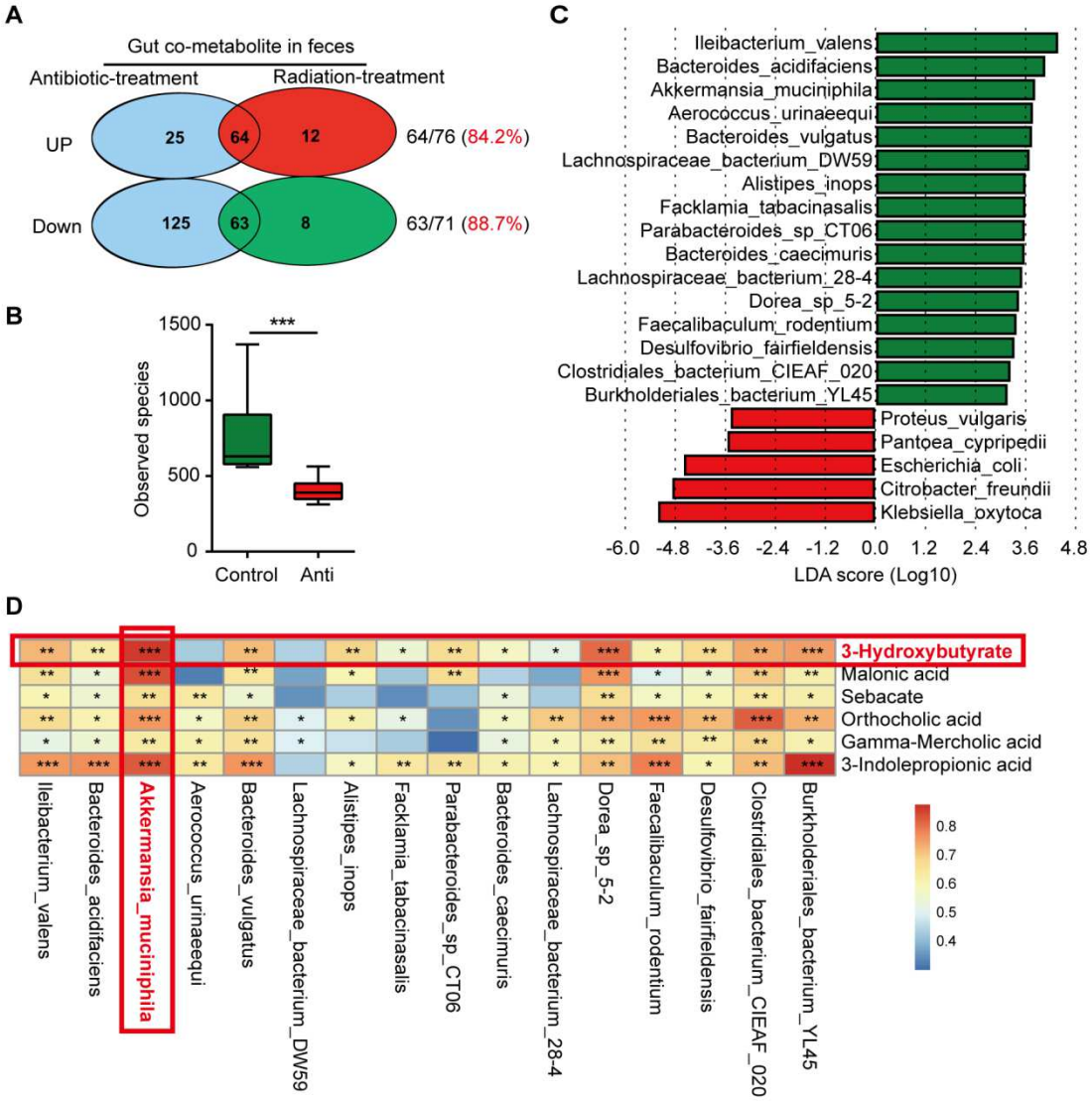

Figure S8. The concentration of 3HB in feces is associated with specific gut bacteria, in particularly with *A. muciniphila* abundance.

(**A**) Venn diagram displays that radiation-induced metabolite profile in feces is similar to that of antibiotic treatment, indicating the same alterations in gut microbiota. (**B**) Observed species in control (Control) and antibiotic-treated (Anti) mice. (**C**) Histogram of the linear discriminant analysis (LDA) coupled with effect size measurements (LEfSe) [LDA significant threshold (log10) > ±3] identified taxonomic biomarkers at species level between Control and Anti groups. Higher abundant species in Control and Anti are shaded in green and red, respectively.

(**D**) Heatmap showing positive and negative correlations between identified taxonomic biomarkers at species level (X axis) and six gut co-metabolites (Y axis) that are different in Control and Anti groups. The boxes in red frame indicate the significantly positive correlation between 3HB and *A. muciniphila*. $*P < 0.05$, $**P < 0.01$, and $***P < 0.001$ determined by Spearman correlation.

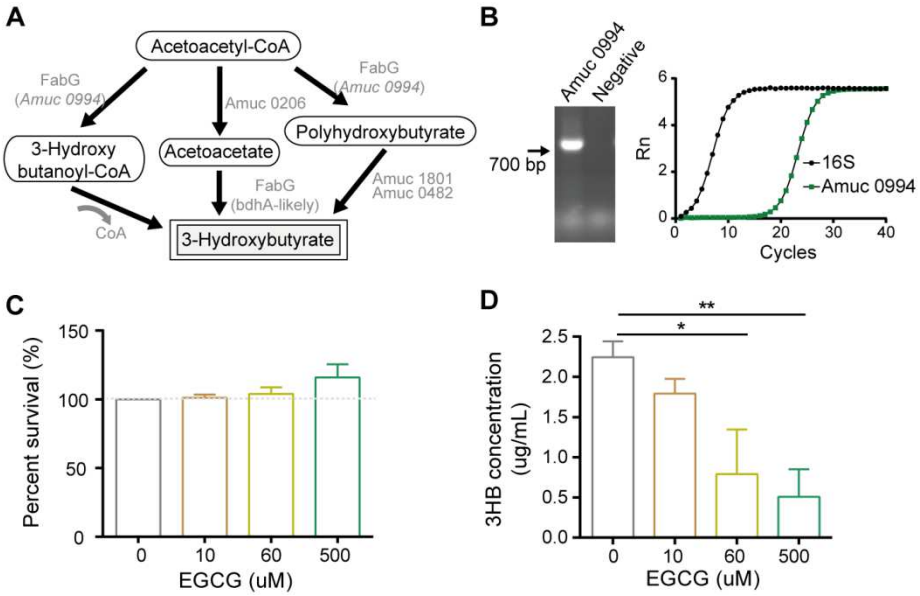

Figure S9. *A. muciniphila* plays a contributing role in accumulating 3HB levels *via* FabG-mediated pathway.

(**A**) Schematic diagram for 3HB biosynthesis pathway in bacteria according to Mierziak *et al*. FabG (Acetoacetyl-CoA reductase) can also function as PhaB.

(**B**) The existence and involvement of *fabG* gene (*Amuc 0994*) in 3HB biosynthesis pathway in *A. muciniphila* was confirmed through the bacterial genomic DNA and bacterial mRNA analysis.

(**C**) Survival of *A. muciniphila* bacteria in stationary phase treated with 0, 10, 60, and 500 uM EGCG for 24 hours.

(**D**) Measurement of 3HB concentration in the supernatant of *A. muciniphila* treated with 0, 10, 60, and 500 uM EGCG for 24 hours.

Data are representative of at least two biological replicates. Data are presented as the mean ± SEM. **P* < 0.05 and ***P* < 0.01 determined by the Student's *t*-test (D).

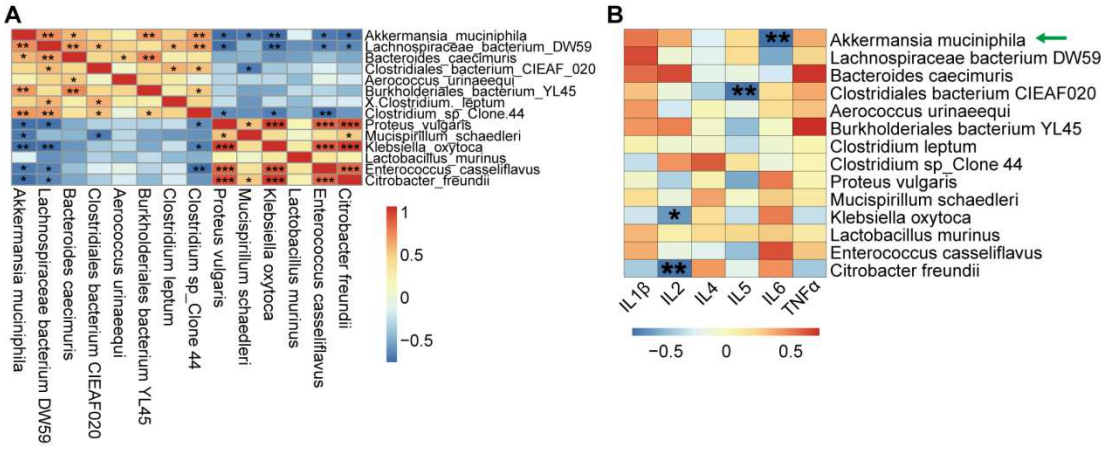

Figure S10. ***A. muciniphila*** **has potential in regulating intestinal homeostasis and downregulating IL6 expression.**

(**A**) Heatmap showing positive (red) and negative (blue) correlations between selected differential bacteria in UR and RP mice.

(**B**) Heatmap showing positive (red) and negative (blue) correlations between bacteria and cytokine concentration measured in the RP mice.

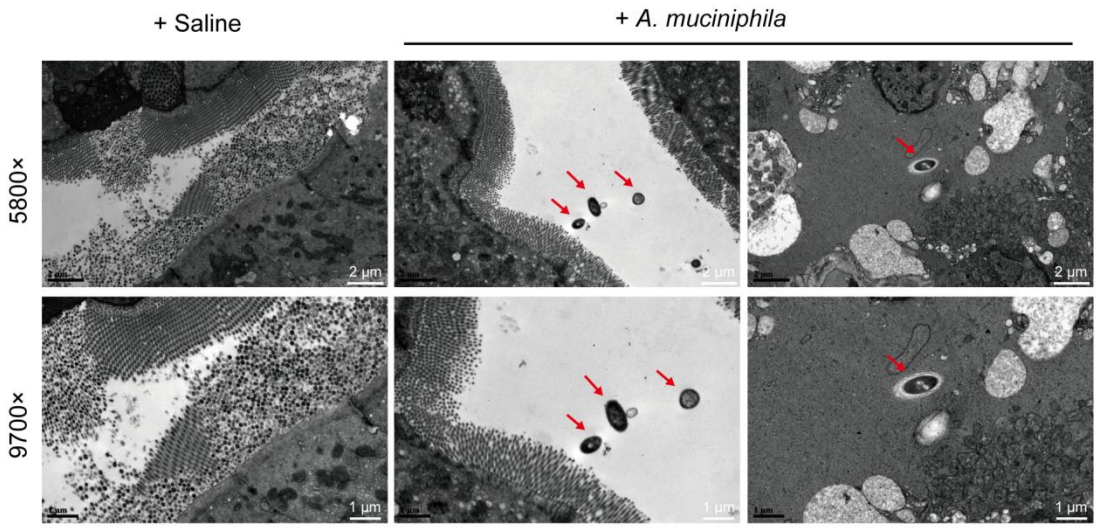

Figure S11. Representative transmission electron micrographs of intestinal samples from RP mice orally administrated with *A. muciniphila* or saline.

Insets in higher magnification are in bottom row. *A. muciniphila* cells in the intestinal lumen and the intestines are observed at the left and the right panels, respectively, in mice orally administrated with *A. muciniphila*. Note that no or very few *A. muciniphila* is observed in mice treated with saline. Scale bars, 2 μm (Top panel) and 1 μm (Bottom panel). Red arrows indicate gut bacteria colonizing the colon tissues.

Supplementary Tables

Table S1. Radiation Injury Score (RIS) Parameters for radiation proctopathy.

Assess the following parameters:	
A. Mucosal ulceration	
	0 = NO ulcerations in mucosa
	1 = Small superficial ulcerations
	2 = Ulcerations involving submucosa
B. Inflammatory cell infiltrate	
	0 = Normal
	1 = Increased density of inflammation cells with focal aggregation in mucosa or submucosa
	2 = Multi-focal aggregation of inflammatory cells in mucosa or submucosa
C. Edema	
	0 = NO edema
	1 = Edema
D. Vascular stenosis	
	0 = Normal
	1 = 25% - 49% stenosis
	2 = 50% - 75% stenosis
	3 = More than 75% stenosis
E. Submucosa fibrosis	
	0 = Normal
	1 = Mild increase in collagen fibers
	2 = Dense fibers were significantly increased, and the vessel wall was hyaline degeneration

Table S2. The significant expressed metabolites in serum between RP and UR (RP to UR)

Formula	Compounds	VIP	P value	Fold Change	Log2FC (RP/UR)	Type
C6H12O5	1,5-Anhydro-D-Glucitol	2.38	0.00007	0.18	-2.48	down
C6H12O5	L-Fucose	2.38	0.00007	0.18	-2.48	down
C6H12O5	L-Rhamnose	2.38	0.00007	0.18	-2.48	down
C4H8O3	3-Hydroxybutyrate	2.40	0.00016	0.12	-3.12	down
C3H4O4	Malonicacid	2.38	0.00017	0.12	-3.10	down
C4H7NO3	N-Acetylglycine	2.03	0.00114	0.49	-1.02	down
C11H11NO3	N-Cinnamylglycine	2.05	0.00148	2.31	1.21	up
C8H15NO3	Hexanoyl Glycine	2.24	0.00042	0.20	-2.30	down
C10H13N5O5	Guanosine	2.34	0.00005	0.41	-1.28	down
C10H9NO3	5-Hydroxyindole-3-Acetic Acid	1.99	0.00202	2.73	1.45	up
C10H12N2O4	3-Hydroxykynurenine	2.45	0.00008	0.25	-1.97	down
C13H25NO4	Hexanoylcarnitine	2.13	0.00200	0.30	-1.72	down
C23H43NO4	Carnitine C16:1	2.02	0.00178	0.45	-1.14	down
C23H41NO4	Carnitine C16:2	2.21	0.00034	0.47	-1.09	down
C22H41NO4	Carnitine C15:1	2.17	0.00114	0.45	-1.16	down
C21H39NO4	Carnitine C14:1	1.99	0.00177	0.44	-1.17	down
C21H37NO4	Carnitine C14:2	2.12	0.00148	0.43	-1.22	down
C20H37NO4	Carnitine C13:1	2.17	0.00093	0.42	-1.24	down
C13H25NO4	Carnitine C6:0 Isomer 2	2.13	0.00200	0.30	-1.72	down
C13H25NO4	Carnitine C6:0 Isomer 1	2.13	0.00126	0.31	-1.68	down
C13H25NO4	Carnitine C6:0	2.13	0.00200	0.30	-1.72	down
C21H37NO4	Carnitine C14:2 Isomer 1	2.15	0.00175	0.42	-1.27	down
C23H41NO4	Carnitine C16:2 Isomer1	2.24	0.00032	0.46	-1.13	down
C21H35NO6	Carnitine C14:2:DC	2.03	0.00124	0.46	-1.13	down

Table S3. The significant expressed metabolites in feces between RP and UR (RP to UR)

Formula	Compounds	VIP	P value	Fold Change	Log2FC (RP/UR)	Type
C6H13N3O3	L-Citrulline	1.44	0.00620	0.256	-1.97	down
C9H8O4	4-Hydroxyphenylpyruvic Acid	1.11	0.03252	0.146	-2.77	down
C11H20N2O6	L-Saccharopine	1.39	0.00730	4.752	2.25	up
C13H16N2O4	Phenylacetyl-L-Glutamine	1.34	0.01802	2.505	1.32	up
C3H7NO5S2	S-Sulfo-L-Cysteine	1.19	0.04188	5.786	2.53	up
C6H5NO2	2-Picolinic Acid	1.45	0.02000	0.470	-1.09	down
C5H4N4O2	Xanthine	1.20	0.02965	0.457	-1.13	down
C9H12N2O5	2'-Deoxyuridine	1.29	0.01142	0.274	-1.87	down
C10H13N5O6	8-Hydroxyguanosine	1.09	0.04069	3.231	1.69	up
C9H14N3O8P	Cytidine-5-Monophosphate	1.33	0.00484	0.418	-1.26	down
C27H33N9O15P2	Flavin Adenine Dinucleotide	1.25	0.02747	0.299	-1.74	down
C5H4N4O	Hypoxanthine	1.51	0.01386	0.355	-1.49	down
C10H14N2O5	Thymidine	1.18	0.03644	0.365	-1.45	down
C15H12I3NO4	3,3',5-Triiodo-L-Thyronine	1.43	0.00270	0.367	-1.45	down
C5H6O5	A-Ketoglutaric Acid	1.58	0.00908	0.125	-3.00	down
C6H12O6	D-Glucose	1.05	0.02573	2.279	1.19	up
C18H32O16	D-Melezitose	1.18	0.01569	2.752	1.46	up
C18H32O16	Maltotriose	1.18	0.01569	2.752	1.46	up
C27H44O	Vitamin D3	1.47	0.00230	0.178	-2.49	down
C9H17NO5	Pantothenate	1.25	0.03200	0.409	-1.29	down
C9H7NO2	Indole-2-Carboxylic Acid	1.11	0.01664	0.070	-3.83	down
C5H8O4	2-Methylsuccinic Acid	1.31	0.01042	0.281	-1.83	down
C4H8O3	3-Hydroxybutyrate	1.69	0.00249	0.116	-3.10	down
C9H16O4	Azelaic Acid	1.49	0.00361	0.399	-1.33	down
C12H22O4	Dodecanedioic Aicd	1.44	0.00899	0.190	-2.40	down
C5H8O4	Glutaric Acid	1.31	0.01042	0.281	-1.83	down
C3H9N3O3S	Guanidinoethyl Sulfonate	1.23	0.01161	3.896	1.96	up
C9H10O2	Hydrocinnamic Acid	1.28	0.01665	0.226	-2.14	down
C4H6O6	L-Tartaric Acid	1.35	0.04232	4.781	2.26	up
C3H4O4	Malonicacid	1.68	0.00231	0.119	-3.07	down
C10H18O4	Sebacate	1.33	0.00944	0.294	-1.77	down
C8H14O4	Subericacid	1.24	0.02053	0.442	-1.18	down
C20H32O5	LipoxinA4 [5S,6R,15S-trihydroxy-7E,9E,11Z,13E-eicosatetraenoic acid]	1.22	0.01443	0.371	-1.43	down
C20H34O2	Cis-11,14,17-Eicosatrienoic Acid(C20:3)	1.27	0.04072	0.434	-1.20	down
C20H40O2	Arachidic Acid(C20:0)	1.31	0.01330	0.324	-1.63	down
C5H8O4	Ethylmalonate	1.31	0.01042	0.281	-1.83	down
C12H17N5O5	2-(Dimethylamino)Guanosine	1.42	0.01703	4.838	2.27	up
C6H12O3	5-Hydroxyhexanoic Acid	1.24	0.02507	0.362	-1.47	down
C10H13N5O5	8-Hydroxy-2-Deoxyguanosine	1.37	0.02962	3.411	1.77	up

C9H12N2O6	B-Pseudouridine	1.61	0.02294	0.149	-2.75	down
C6H8O5	Oxoadipic Acid	1.24	0.01557	0.284	-1.82	down
C5H10O2	Valeric Acid	1.44	0.01103	0.261	-1.94	down
C5H8O3	3-Methyl-2-Oxobutanoic Acid	1.27	0.01594	0.190	-2.40	down
C11H11NO3	Indole-3-lactic acid	1.79	0.00351	3.352	1.75	up
C6H10O8	D-Glucarate	1.16	0.03119	4.009	2.00	up
C10H12N4O6	Xanthosine	1.30	0.03727	0.282	-1.82	down
C20H32O6	6-Ketoprostaglandin E1	1.16	0.04539	5.393	2.43	up
C5H9NO3	N-Acetyl-L-alanine	1.15	0.02409	2.206	1.14	up
C9H15N2O15P3	Uridine triphosphate(UTP)	1.17	0.03781	7.773	2.96	up
C18H34O3	Ricinoleic acid	1.03	0.04533	0.441	-1.18	down
C20H34O4	5,6-DiHETrE [(±)5,6-dihydroxy-8Z,11Z,14Z-eicosatrienoic acid]	1.08	0.04002	0.469	-1.09	down
C20H34O5	5-iPF2α-VI [(8β)-5,9α,11α-trihydroxy-prosta-6E,14Z-dien-1-oic acid]	1.13	0.01101	0.340	-1.56	down
C20H32O5	Prostaglandin E2	1.17	0.04554	9.426	3.24	up
C5H9NO3	N-acetyl-beta-alanine	1.18	0.02353	2.221	1.15	up
C15H12I3NO4	3,3',5'-Triiodothyronine	1.43	0.00270	0.367	-1.45	down
C26H43NO5	Glycine deoxycholic acid	1.22	0.04484	0.274	-1.87	down
C18H32O4	13-HpODE	1.31	0.01450	0.331	-1.60	down
C6H12O3	2-ethyl-2-hydroxybutyric acid	1.25	0.02073	0.352	-1.51	down
C24H38O4	7-ketolithocholic acid	1.20	0.00585	0.253	-1.98	down
C13H24O4	1,11-undecylic acid	1.32	0.02050	0.381	-1.39	down
C16H32O3	16-Hydroxyhexadecanoic acid	1.36	0.00677	0.338	-1.56	down
C24H38O4	12-ketolithocholic acid	1.20	0.00585	0.253	-1.98	down
C19H40O3	Heparin	1.53	0.00140	0.208	-2.26	down
C24H38O4	Orthocholic acid	1.20	0.00430	0.233	-2.10	down
C9H7NO2	Indole-3-carboxylic acid	1.39	0.04221	0.235	-2.09	down
C6H10O3	4-methyl-2-oxovaleric acid	1.27	0.01559	0.239	-2.07	down
C10H13NO6S	L-tyrosine methyl ester 4-sulfate	1.20	0.02523	4.851	2.28	up
C5H9NO3	2-amino-4-oxovaleric acid	1.18	0.02353	2.221	1.15	up
C10H11NO4	P-hydroxyphenylacetylglycine	1.09	0.02861	2.984	1.58	up
C7H11NO5	L-2-amino-6-oximelic acid	1.44	0.01650	0.291	-1.78	down
C6H10O8	Mucic Acid	1.15	0.03004	4.478	2.16	up
C3H7NO2	L-Alanine	1.78	0.00068	0.357	-1.49	down
C9H10INO3	3-Iodo-L-Tyrosine	1.17	0.02436	8.275	3.05	up
C11H12N2O3	5-Hydroxy-L-Tryptophan	1.03	0.02035	5.944	2.57	up
C5H7NO3	5-Oxoproline	1.29	0.01309	0.398	-1.33	down
C6H9NO5	N-Acetylaspartate	1.65	0.00523	4.311	2.11	up
C7H11NO5	N-Acetyl-L-Glutamic Acid	1.24	0.00672	0.208	-2.26	down
C8H15NO6	N-Acetylmannosamine	1.21	0.01537	0.379	-1.40	down
C5H14NO+	Choline	1.39	0.04739	2.800	1.49	up
C5H6N2O2	Thymine	1.50	0.01806	0.236	-2.08	down

C15H11I4NO4	L-Thyroxine	1.25	0.02398	0.260	-1.94	down
C10H12N2	Tryptamine	1.37	0.01332	0.013	-6.24	down
C6H5NO2	Nicotinic Acid	1.50	0.00395	0.361	-1.47	down
C17H20N4O6	Riboflavin	1.25	0.01547	0.482	-1.05	down
C4H7N3O	Creatinine	1.53	0.02293	6.422	2.68	up
C13H16N2O4	N-γ-Acetyl-N-2-Formyl-5-Methoxykynurenamine	1.85	0.00032	3.570	1.84	up
C9H11N5O3	Biopterin	1.47	0.02550	3.458	1.79	up
C8H12NO6P	Pyridoxine 5'-Phosphate	1.54	0.01343	0.219	-2.19	down
C6H11NO2	DL-Pipecolic Acid	1.35	0.00825	0.385	-1.38	down
C10H7NO4	Xanthurenic Acid	1.57	0.00349	0.203	-2.30	down
C6H11NO4	2-Aminoadipic Acid	1.41	0.00999	0.489	-1.03	down
C20H23N7O7	10-Formyl-Thf	1.65	0.00502	7.241	2.86	up
C6H13NO2	L-Norleucine	1.79	0.00430	2.666	1.41	up
C10H10N2O	Indole-3-acetamide	1.42	0.01916	5.036	2.33	up
C18H28O2	Stearidonic Acid	1.26	0.03314	0.415	-1.27	down
C12H23NO4	2-Methylbutyroylcarnitine	1.51	0.01147	4.287	2.10	up
C21H42NO7P	LysoPE(16:1(9Z)/0:0)	1.56	0.03205	2.265	1.18	up
C6H10N2O4	N-Alpha-Acetyl-L-Asparagine	1.41	0.01755	3.602	1.85	up
C3H7NO2	β-Alanine	1.78	0.00068	0.357	-1.49	down
C33H34N4O6	Biliverdin	1.47	0.00799	3.259	1.70	up
C13H15N3O3	Glycyl-tryptophan	1.38	0.03965	3.002	1.59	up
C5H4N4O2	Oxypurinol	1.47	0.00125	0.270	-1.89	down
C19H37NO4	Dodecylcarnitine	1.62	0.01302	5.845	2.55	up
C17H33NO4	Decanoyl L-Carnitine	1.49	0.04753	7.966	2.99	up
C24H40O3	Lithocholic acid	1.20	0.01503	0.213	-2.23	down
C15H12O5	(-)-Norepinephrine	1.72	0.00200	3.994	2.00	up
C20H30O2	5,6-dehydroarachidonic acid	1.23	0.04213	0.164	-2.61	down
C21H41NO4	(±) -Myristylcarnitine	1.44	0.02032	3.745	1.90	up
C20H23N7O7	Folic acid	1.65	0.00502	7.241	2.86	up
C33H42N4O6	Urobilin	1.21	0.02975	0.353	-1.50	down
C13H25NO4	Hexanoylcarnitine	1.40	0.04836	4.791	2.26	up
C12H16N2O4	Alanine tyrosine	1.47	0.00136	0.144	-2.80	down
C25H45NO5	Carnitine C18:2-OH	1.72	0.00651	3.373	1.75	up
C25H45NO4	Carnitine C18:2	1.34	0.03225	2.072	1.05	up
C25H43NO4	Carnitine C18:3	1.36	0.02650	2.889	1.53	up
C25H41NO4	Carnitine C18:4	1.67	0.01768	6.272	2.65	up
C22H39NO6	Carnitine C15:1:DC	1.62	0.00440	16.743	4.07	up
C23H43NO4	Carnitine C16:1	1.50	0.01568	2.896	1.53	up
C23H41NO4	Carnitine C16:2	1.51	0.01866	7.723	2.95	up
C23H39NO4	Carnitine C16:3	1.53	0.01561	5.221	2.38	up
C21H41NO5	Carnitine C14-OH	1.75	0.00514	3.433	1.78	up
C21H39NO5	Carnitine C14:1-OH	1.34	0.00328	6.599	2.72	up
C22H41NO4	Carnitine C15:1	1.20	0.01203	4.757	2.25	up
C21H37NO5	Carnitine C14:2-OH	1.59	0.01481	12.059	3.59	up

C21H41NO4	Carnitine C14:0	1.42	0.01798	3.991	2.00	up
C21H39NO4	Carnitine C14:1	1.61	0.00867	6.792	2.76	up
C21H37NO4	Carnitine C14:2	1.31	0.02474	7.756	2.96	up
C21H35NO4	Carnitine C14:3	1.40	0.04707	10.653	3.41	up
C19H37NO5	Carnitine C12-OH	1.49	0.00576	5.981	2.58	up
C18H33NO6	Carnitine C11:DC	1.49	0.00609	5.844	2.55	up
C20H39NO4	Carnitine C13:0	1.80	0.00478	5.668	2.50	up
C20H37NO4	Carnitine C13:1	1.72	0.00338	2.987	1.58	up
C19H35NO4	Carnitine C12:1	1.65	0.01253	7.877	2.98	up
C18H35NO4	Carnitine C11:0	1.24	0.00926	6.785	2.76	up
C18H33NO4	Carnitine C11:1	1.74	0.02537	10.002	3.32	up
C17H33NO4	Carnitine C10:0	1.53	0.04268	7.760	2.96	up
C15H29NO5	Carnitine C8-OH	1.41	0.02806	4.641	2.21	up
C16H31NO4	Carnitine C9:0	1.90	0.01021	6.693	2.74	up
C15H27NO4	Carnitine C8:1	1.51	0.02298	9.103	3.19	up
C13H25NO4	Carnitine C6:0	1.40	0.04836	4.791	2.26	up
C12H23NO4	Carnitine C5:0	1.50	0.00995	4.235	2.08	up
C8H15NO6	N-Acetyl-D-Galactosamine	1.15	0.01998	0.451	-1.15	down
C4H4N6O	8-Azaguanine	1.47	0.00355	0.271	-1.88	down
C19H31NO4	Carnitine C12:3	1.42	0.01414	6.831	2.77	up
C21H35NO6	Carnitine C14:2:DC	1.48	0.01660	2.838	1.50	up
C23H41NO5	Carnitine C16:2-OH	1.54	0.00357	7.769	2.96	up
C23H41NO5	Carnitine C16:2-OH Isomer 1	1.67	0.00243	7.700	2.94	up

Table S4. **The details of correlation between serum and fecal metabolites measured in the RP mice.**

Spearman correlation between serum and fecal metabolites measured in the RP mice.

	Carnitine C15:1:DC	Carnitine C14:2-OH	Carnitine C14:3	Carnitine C11:1	Prostaglandin E2	Carnitine C8:1	3-Iodo-L-Tyrosine	Decanoyl L-Carnitine	Carnitine C12:1	Uridine triphosphate
5-Hydroxyindole-3-Acetic Acid	R = 0.45 *P* = 0.26	R = 0.45 *P* = 0.26	R = 0.50 *P* = 0.20	R = 0.38 *P* = 0.35	R = -0.21 *P* = 0.61	R = 0.76 *P* = 0.02	R = 0.24 *P* = 0.56	R = 0.59 *P* = 0.11	R = 0.69 *P* = 0.06	R = -0.14 *P* = 0.72
N-Cinnamylglycine	R = 0.42 *P* = 0.28	R = 0.57 *P* = 0.13	R = 0.65 *P* = 0.07	R = 0.40 *P* = 0.31	R = 0.07 *P* = 0.86	R = 0.73 *P* = 0.03	R = 0.34 *P* = 0.40	R = 0.76 *P* = 0.02	R = 0.78 *P* = 0.02	R = -0.04 *P* = 0.90
Carnitine C16:1	R = 0.21 *P* = 0.61	R = 0.02 *P* = 0.95	R = -0.04 *P* = 0.91	R = 0.14 *P* = 0.73	R = 0.26 *P* = 0.53	R = 0 *P* = 1	R = 0.04 *P* = 0.90	R = -0.11 *P* = 0.77	R = -0.21 *P* = 0.61	R = 0.24 *P* = 0.56
Carnitine C15:1	R = -0.07 *P* = 0.86	R = 0.02 *P* = 0.95	R = -0.17 *P* = 0.67	R = -0.11 *P* = 0.77	R = 0.19 *P* = 0.65	R = -0.02 *P* = 0.95	R = -0.26 *P* = 0.52	R = -0.11 *P* = 0.77	R = -0.21 *P* = 0.61	R = -0.07 *P* = 0.86
Carnitine C14:1	R = -0.09 *P* = 0.82	R = -0.23 *P* = 0.57	R = -0.32 *P* = 0.43	R = -0.14 *P* = 0.73	R = 0.21 *P* = 0.61	R = -0.33 *P* = 0.41	R = -0.17 *P* = 0.68	R = -0.38 *P* = 0.35	R = -0.52 *P* = 0.18	R = -0.02 *P* = 0.95
Carnitine C14:2	R = -0.07 *P* = 0.86	R = -0.35 *P* = 0.38	R = -0.41 *P* =0.30	R = -0.23 *P* = 0.57	R = 0.04 *P* = 0.91	R = -0.30 *P* = 0.45	R = -0.26 *P* = 0.52	R = -0.45 *P* = 0.26	R = -0.57 *P* = 0.13	R = -0.02 *P* = 0.95
Carnitine C13:1	R = 0.09 *P* = 0.82	R = -0.23 *P* = 0.57	R = -0.14 *P* = 0.73	R = -0.19 *P* = 0.65	R = 0.04 *P* = 0.91	R = -0.02 *P* = 0.95	R = -0.14 *P* = 0.72	R = -0.09 *P* = 0.82	R = -0.26 *P* = 0.53	R = -0.19 *P* = 0.64
Carnitine C14:2 Isomer 1	R = -0.07 *P* = 0.86	R = -0.35 *P* = 0.38	R = -0.41 *P* = 0.30	R = -0.23 *P* = 0.57	R = 0.04 *P* = 0.91	R = -0.30 *P* = 0.45	R = -0.26 *P* = 0.52	R = -0.45 *P* = 0.26	R = -0.57 *P* = 0.13	R = -0.02 *P* = 0.95
Guanosine	R = -0.19 *P* = 0.65	R = -0.38 *P* = 0.35	R = -0.41 *P* = 0.30	R = -0.19 *P* = 0.65	R = -0.02 *P* = 0.95	R = -0.50 *P* = 0.20	R = -0.12 *P* = 0.77	R = -0.52 *P* = 0.18	R = -0.50 *P* = 0.20	R = 0.31 *P* = 0.44
Carnitine C6:0 Isomer 1	R = -0.30 *P* = 0.45	R = -0.40 *P* = 0.31	R = -0.49 *P* = 0.21	R = -0.28 *P* = 0.49	R = 0.14 *P* = 0.73	R = -0.59 *P* = 0.11	R = -0.26 *P* = 0.52	R = -0.59 *P* = 0.11	R = -0.71 *P* = 0.04	R = -0.02 *P* = 0.95
Carnitine C6:0	R = -0.28 *P* = 0.49	R = -0.33 *P* = 0.41	R = -0.46 *P* = 0.24	R = -0.21 *P* = 0.61	R = 0.16 *P* = 0.69	R = -0.54 *P* = 0.16	R = -0.24 *P* = 0.56	R = -0.57 *P* = 0.13	R = -0.69 *P* = 0.06	R = -0.09 *P* = 0.81
3-Hydroxykynurenine	R = -0.04 *P* = 0.91	R = 0 *P* = 1	R = -0.07 *P* = 0.86	R = 0.04 *P* = 0.91	R = 0.33 *P* = 0.41	R = -0.28 *P* = 0.49	R = -0.12 *P* = 0.77	R = -0.14 *P* = 0.73	R = -0.11 *P* = 0.77	R = 0.65 *P* = 0.07
3-Hydroxybutyrate	R = -0.35 *P* = 0.38	R = -0.30 *P* = 0.45	R = -0.40 *P* = 0.31	R = -0.42 *P* = 0.28	R = 0.07 *P* = 0.86	R = -0.40 *P* = 0.31	R = -0.39 *P* = 0.33	R = -0.35 *P* = 0.38	R = -0.42 *P* = 0.28	R = 0 *P* = 1
Hexanoyl Glycine	R = 0.09 *P* = 0.82	R = -0.04 *P* = 0.91	R = -0.23 *P* = 0.56	R = -0.02 *P* = 0.95	R = -0.57 *P* = 0.13	R = 0.33 *P* = 0.41	R = -0.31 *P* = 0.44	R = -0.14 *P* = 0.73	R = -0.04 *P* = 0.91	R = -0.60 *P* = 0.10

L-Rhamnose	R = -0.23 *P* = 0.57	R = -0.14 *P* = 0.73	R = -0.27 *P* = 0.50	R = -0.30 *P* = 0.45	R = 0.07 *P* = 0.86	R = -0.16 *P* = 0.69	R = -0.36 *P* = 0.37	R = -0.19 *P* = 0.65	R = -0.28 *P* = 0.49	R = -0.21 *P* = 0.60
L-Fucose	R = -0.23 *P* = 0.57	R = -0.14 *P* = 0.73	R = -0.27 *P* = 0.50	R = -0.30 *P* = 0.45	R = 0.07 *P* = 0.86	R = -0.16 *P* = 0.69	R = -0.36 *P* = 0.37	R = -0.19 *P* = 0.65	R = -0.28 *P* = 0.49	R = -0.21 *P* = 0.60
1,5-Anhydro-D-Glucitol	R = -0.23 *P* = 0.57	R = -0.14 *P* = 0.73	R = -0.27 *P* = 0.50	R = -0.30 *P* = 0.45	R = 0.07 *P* = 0.86	R = -0.16 *P* = 0.69	R = -0.36 *P* = 0.37	R = -0.19 *P* = 0.65	R = -0.28 *P* = 0.49	R = -0.21 *P* = 0.60
Malonicacid	R = -0.19 *P* = 0.65	R = -0.19 *P* = 0.65	R = -0.25 *P* = 0.54	R = -0.28 *P* = 0.49	R = 0.11 *P* = 0.77	R = -0.23 *P* = 0.57	R = -0.24 *P* = 0.56	R = -0.19 *P* = 0.65	R = -0.26 *P* = 0.53	R = 0.04 *P* = 0.90
Carnitine C6:0 Isomer 2	R = -0.28 *P* = 0.49	R = -0.33 *P* = 0.41	R = -0.46 *P* = 0.24	R = -0.21 *P* = 0.61	R = 0.16 *P* = 0.69	R = -0.54 *P* = 0.16	R = -0.24 *P* = 0.56	R = -0.57 *P* = 0.13	R = -0.69 *P* =0.06	R = -0.09 *P* = 0.81
Hexanoylcarnitine	R = -0.28 *P* = 0.49	R = -0.33 *P* = 0.41	R = -0.46 *P* = 0.24	R = -0.21 *P* = 0.61	R = 0.16 *P* = 0.69	R = -0.54 *P* = 0.16	R = -0.24 *P* = 0.56	R = -0.57 *P* = 0.13	R = -0.69 *P* = 0.06	R = -0.09 *P* = 0.81

	Vitamin D3	5,6-dehydroarachidonic acid	B-Pseudouridine	4-Hydroxyphenylpyruvic Acid	Alanine tyrosine	A-Ketoglutaric Acid	Malonicacid	Indole-2-Carboxylic Acid	Tryptamine	3-Hydroxybutyrate
5-Hydroxyindole-3-Acetic Acid	R = -0.40 *P* = 0.31	R = -0.27 *P* = 0.51	R = -0.26 *P* = 0.53	R = -0.05 *P* = 0.89	R = 0.09 *P* = 0.82	R = -0.30 *P* = 0.45	R = -0.80 *P* = 0.02	R = -0.10 *P* = 0.79	R = -0.07 *P* = 0.86	R = -0.69 *P* = 0.06
N-Cinnamylglycine	R = -0.48 *P* = 0.22	R = -0.43 *P* = 0.27	R = -0.40 *P* = 0.31	R = -0.32 *P* = 0.42	R = -0.29 *P* = 0.47	R = -0.42 *P* = 0.28	R = -0.47 *P* = 0.23	R = -0.30 *P* = 0.47	R = -0.42 *P* = 0.28	R = -0.26 *P* = 0.53
Carnitine C16:1	R = -0.43 *P* = 0.27	R = -0.21 *P* = 0.60	R = -0.02 *P* = 0.95	R = 0.10 *P* = 0.79	R = 0.34 *P* = 0.40	R = 0.30 *P* = 0.45	R = 0 *P* = 1	R = 0 *P* = 1	R = 0.16 *P* = 0.69	R = -0.02 *P* = 0.95
Carnitine C15:1	R = -0.20 *P* = 0.63	R = 0 *P* = 1	R = 0.23 *P* = 0.57	R = 0.10 *P* = 0.79	R = -0.07 *P* = 0.85	R = 0.23 *P* = 0.57	R = 0.40 *P* = 0.31	R = 0.19 *P* = 0.65	R = 0.04 *P* = 0.91	R = 0.66 *P* = 0.07
Carnitine C14:1	R = -0.01 *P* = 0.97	R = 0.10 *P* = 0.79	R = 0.30 *P* = 0.45	R = 0.21 *P* = 0.60	R = 0.23 *P* = 0.57	R = 0.45 *P* = 0.26	R = 0.30 *P* = 0.45	R = 0.19 *P* = 0.65	R = 0.26 *P* = 0.53	R = 0.35 *P* = 0.38
Carnitine C14:2	R = -0.01 *P* = 0.97	R = 0.19 *P* = 0.65	R = 0.35 *P* = 0.38	R = 0.35 *P* = 0.38	R = 0.34 *P* = 0.40	R = 0.57 *P* = 0.13	R = 0.33 *P* = 0.41	R = 0.32 *P* = 0.42	R = 0.38 *P* = 0.35	R = 0.33 *P* = 0.41
Carnitine C13:1	R = -0.09 *P* = 0.82	R = 0.10 *P* = 0.79	R = 0.28 *P* = 0.49	R = 0.21 *P* = 0.60	R = 0.06 *P* = 0.88	R = 0.47 *P* = 0.23	R = 0.30 *P* = 0.45	R = 0.27 *P* = 0.51	R = 0.14 *P* = 0.73	R = 0.45 *P* = 0.26
Carnitine C14:2 Isomer 1	R = -0.01 *P* = 0.97	R = 0.19 *P* = 0.65	R = 0.35 *P* = 0.38	R = 0.35 *P* = 0.38	R = 0.34 *P* = 0.40	R = 0.57 *P* = 0.13	R = 0.33 *P* = 0.41	R = 0.32 *P* = 0.42	R = 0.38 *P* = 0.35	R = 0.33 *P* = 0.41

Guanosine	R = 0.23 *P* = 0.57	R = 0.19 *P* = 0.65	R = 0.14 *P* = 0.73	R = 0.13 *P* = 0.74	R = 0.15 *P* = 0.71	R = 0.21 *P* = 0.61	R = 0.42 *P* = 0.28	R = 0.10 *P* = 0.79	R = 0.26 *P* = 0.53	R = 0.11 *P* = 0.77
Carnitine C6:0 Isomer 1	R = 0.20 *P* = 0.63	R = 0.24 *P* = 0.55	R = 0.30 *P* = 0.45	R = 0.30 *P* = 0.47	R = 0.40 *P* = 0.31	R = 0.52 *P* = 0.18	R = 0.28 *P* = 0.49	R = 0.21 *P* = 0.60	R = 0.33 *P* = 0.41	R = 0.23 *P* = 0.57
Carnitine C6:0	R = 0.20 *P* = 0.63	R = 0.24 *P* = 0.55	R = 0.38 *P* = 0.35	R = 0.30 *P* = 0.47	R = 0.40 *P* = 0.31	R = 0.47 *P* = 0.23	R = 0.19 *P* = 0.65	R = 0.21 *P* = 0.60	R = 0.38 *P* = 0.35	R = 0.19 *P* = 0.65
3-Hydroxykynurenine	R = -0.06 *P* = 0.88	R = -0.19 *P* = 0.65	R = -0.16 *P* = 0.69	R = -0.35 *P* = 0.38	R = -0.51 *P* = 0.19	R = -0.21 *P* = 0.61	R = 0.83 *P* = 0.02	R = -0.24 *P* = 0.55	R = -0.26 *P* = 0.53	R = 0.59 *P* = 0.11
3-Hydroxybutyrate	R = 0.21 *P* = 0.60	R = 0.24 *P* = 0.55	R = 0.28 *P* = 0.49	R = 0.08 *P* = 0.84	R = -0.29 *P* = 0.47	R = 0.26 *P* = 0.53	R = 0.88 *P* = 0.004	R = 0.24 *P* = 0.55	R = -0.02 *P* = 0.95	R = 0.97 *P* = 3e-05
Hexanoyl Glycine	R = 0.09 *P* = 0.82	R = 0.38 *P* = 0.35	R = 0.57 *P* = 0.13	R = 0.60 *P* = 0.11	R = 0.59 *P* = 0.12	R = 0.21 *P* = 0.61	R = -0.71 *P* = 0.04	R = 0.54 *P* = 0.16	R = 0.73 *P* = 0.03	R = -0.54 *P* = 0.16
L-Rhamnose	R = 0.07 *P* = 0.85	R = 0.19 *P* = 0.65	R = 0.33 *P* = 0.41	R = 0.13 *P* = 0.74	R = -0.18 *P* = 0.65	R = 0.26 *P* = 0.53	R = 0.54 *P* = 0.16	R = 0.27 *P* = 0.51	R = 0.02 *P* = 0.95	R = 0.80 *P* = 0.02
L-Fucose	R = 0.07 *P* = 0.85	R = 0.19 *P* = 0.65	R = 0.33 *P* = 0.41	R = 0.13 *P* = 0.74	R = -0.18 *P* = 0.65	R = 0.26 *P* = 0.53	R = 0.54 *P* = 0.16	R = 0.27 *P* = 0.51	R = 0.02 *P* = 0.95	R = 0.80 *P* = 0.02
1,5-Anhydro-D-Glucitol	R = 0.07 *P* = 0.85	R = 0.19 *P* = 0.65	R = 0.33 *P* = 0.41	R = 0.13 *P* = 0.74	R = -0.18 *P* = 0.65	R = 0.26 *P* = 0.53	R = 0.54 *P* = 0.16	R = 0.27 *P* = 0.51	R = 0.02 *P* = 0.95	R = 0.80 *P* = 0.02
Malonicacid	R = 0.10 *P* = 0.79	R = 0.13 *P* = 0.74	R = 0.23 *P* = 0.57	R = -0.02 *P* = 0.94	R = -0.43 *P* = 0.27	R = 0.14 *P* = 0.73	R = 0.85 *P* = 0.006	R = 0.16 *P* = 0.69	R = -0.09 *P* = 0.82	R = 0.95 *P* = 2e-04
Carnitine C6:0 Isomer 2	R = 0.20 *P* = 0.63	R = 0.24 *P* = 0.55	R = 0.38 *P* = 0.35	R = 0.30 *P* = 0.47	R = 0.40 *P* = 0.31	R = 0.47 *P* = 0.23	R = 0.19 *P* = 0.65	R = 0.21 *P* = 0.60	R = 0.38 *P* = 0.35	R = 0.19 *P* = 0.65
Hexanoylcarnitine	R = 0.20 *P* = 0.63	R = 0.24 *P* = 0.55	R = 0.38 *P* = 0.35	R = 0.30 *P* = 0.47	R = 0.40 *P* = 0.31	R = 0.47 *P* = 0.23	R = 0.19 *P* = 0.65	R = 0.21 *P* = 0.60	R = 0.38 *P* = 0.35	R = 0.19 *P* = 0.65

Table S5. Clinical Score Parameters for radiation proctopathy.

Assess the following parameters and tally with associated scoring system:	
A. Physical appearance	
	0 –normal
	1 – lack of grooming
	2 – rough hair coat
	3 – very rough hair coat
B. Posture	
	0 – normal
	1 – sitting in hunched position
	4 – hunched posture, head resting on floor
	6 – lying prone on cage floor/unable to maintain upright posture (**suggests moribund and euthanasia required)
C. Activity/Behavior	
	0 – normal
	1 – somewhat reduced/minor changes in behavior
	3 – above plus change in respiratory rate or effort
D. Hydration	
	0 – normal
	1 – mildly dehydrated (< 1 sec skin tent)
	2 – moderately dehydrated
	(1-2 sec skin tent)
	3 – severely dehydrated
	(> 2 sec skin tent)
E. Body Weight (assessed every two days)	
	0 – normal (<5% change from initial weight)
	1 – 5-10% weight change
	2 – 10-20% weight change
F. Anal hair (determination of the area of hair loss in the anus)	
	0 – normal
	1 – 0 < area < 1
	2 – 1 < area < 2
	3 – 2< area < 4
Endpoint for euthanasia: any single parameter of 6 or combined score for parameters A to F => 15.	
Immediate endpoints for euthanasia:	
	1. Unconsciousness
	2. Inability to remain upright
	3. Agonal respiration (i.e. gasping)
	4. Convulsions

Table S6. **The details of correlation between bacteria and fecal metabolites that differentially in WT and RP mice.**

Spearman correlation between bacteria and fecal metabolites that differentially in WT and RP mice.

	Akkermansia muciniphila	**Lachnospiraceae bacterium_DW59**	**Bacteroides caecimuris**	**Clostridiales Bacterium CIEAF_020**	**Aerococcus urinaeequi**	**Burkholderiales Bacterium YL45**	**Clostridium leptum**	**Clostridium sp Clone.44**	**Proteus vulgaris**	**Mucispirillum schaedleri**	**Klebsiella oxytoca**	**Lactobacillus murinus**	**Enterococcus casseliflavus**	**Citrobacter freundii**
Carnitine C15:1:DC	R = -0.72 *P* = 1.5e-03	R = -0.58 *P* = 0.02	R = -0.65 *P* = 0.006	R = -0.46 *P* = 0.07	R = -0.41 *P* = 0.11	R = -0.62 *P* = 0.02	R = -0.40 *P* = 0.12	R = -0.50 *P* = 0.04	R = 0.45 *P* = 0.08	R = 0.64 *P* = 0.007	R = 0.41 *P* = 0.11	R = 0.30 *P* = 0.25	R = 0.31 *P* = 0.24	R = 0.39 *P* = 0.13
Carnitine C14:2-OH	R = -0.68 *P* = 3.5e-03	R = -0.46 *P* = 0.07	R = -0.45 *P* = 0.08	R = -0.50 *P* = 0.04	R = -0.20 *P* = 0.46	R = -0.51 *P* = 0.04	R = -0.45 *P* = 0.08	R = -0.57 *P* = 0.02	R = 0.53 *P* = 0.03	R = 0.73 *P* = 0.002	R = 0.43 *P* = 0.09	R = 0.10 *P* = 0.71	R = 0.27 *P* = 0.31	R = 0.40 *P* = 0.12
Carnitine C14:3	R = -0.60 *P* = 1.3e-02	R = -0.43 *P* = 0.10	R = -0.44 *P* = 0.08	R = -0.41 *P* = 0.11	R = -0.08 *P* = 0.77	R = -0.35 *P* = 0.18	R = -0.46 *P* = 0.07	R = -0.38 *P* = 0.15	R = 0.36 *P* = 0.17	R = 0.51 *P* = 0.04	R = 0.30 *P* = 0.26	R = 0.13 *P* = 0.62	R = 0.21 *P* = 0.42	R = 0.26 *P* = 0.34
Carnitine C11:1	R = -0.70 *P* = 2.2e-03	R = -0.61 *P* = 0.01	R = -0.57 *P* = 0.02	R = -0.52 *P* = 0.03	R = -0.13 *P* = 0.62	R = -0.47 *P* = 0.06	R = -0.51 *P* = 0.04	R = -0.60 *P* = 0.014	R = 0.58 *P* = 0.02	R = 0.65 *P* = 0.006	R = 0.56 *P* = 0.02	R = 0.21 *P* = 0.42	R = 0.43 *P* = 0.09	R = 0.53 *P* = 0.03
Prostaglandin E2	R = -0.55 *P* = 2.5e-02	R = -0.35 *P* = 0.18	R = -0.41 *P* = 0.11	R = -0.60 *P* = 0.02	R = -0.24 *P* = 0.37	R = -0.55 *P* = 0.03	R = -0.39 *P* = 0.13	R = -0.40 *P* = 0.12	R = 0.43 *P* = 0.09	R = 0.58 *P* = 0.02	R = 0.42 *P* = 0.10	R = -0.06 *P* = 0.83	R = 0.14 *P* = 0.60	R = 0.34 *P* = 0.20
Carnitine C8:1	R = -0.54 *P* = 2.9e-02	R = -0.47 *P* = 0.06	R = -0.46 *P* = 0.07	R = -0.35 *P* = 0.18	R = -0.03 *P* = 0.92	R = -0.31 *P* = 0.24	R = -0.38 *P* = 0.14	R = -0.48 *P* = 0.06	R = 0.33 *P* = 0.20	R = 0.55 *P* = 0.03	R = 0.30 *P* = 0.26	R = 0.29 *P* = 0.28	R = 0.35 *P* = 0.17	R = 0.30 *P* = 0.25
3-Iodo-L-Tyrosine	R = -0.55 *P* = 2.5e-02	R = -0.40 *P* = 0.13	R = -0.44 *P* = 0.09	R = -0.52 *P* = 0.04	R = -0.07 *P* = 0.79	R = -0.33 *P* = 0.21	R = -0.46 *P* = 0.07	R = -0.26 *P* = 0.32	R = 0.39 *P* = 0.14	R = 0.51 *P* = 0.04	R = 0.35 *P* = 0.18	R = 0.04 *P* = 0.87	R = 0.13 *P* = 0.63	R = 0.33 *P* = 0.20
Decanoyl L-Carnitine	R = -0.69 *P* = 2.8e-03	R = -0.48 *P* = 0.06	R = -0.53 *P* = 0.03	R = -0.54 *P* = 0.03	R = -0.24 *P* = 0.38	R = -0.57 *P* = 0.02	R = -0.48 *P* = 0.06	R = -0.54 *P* = 0.03	R = 0.39 *P* = 0.13	R = 0.69 *P* = 0.003	R = 0.37 *P* = 0.16	R = 0.20 *P* = 0.46	R = 0.31 *P* = 0.24	R = 0.31 *P* = 0.24
Carnitine C12:1	R = -0.70 *P* = 2.4e-03	R = -0.50 *P* = 0.04	R = -0.51 *P* = 0.04	R = -0.47 *P* = 0.07	R = -0.31 *P* = 0.24	R = -0.55 *P* = 0.03	R = -0.51 *P* = 0.04	R = -0.54 *P* = 0.03	R = 0.42 *P* = 0.10	R = 0.69 *P* = 0.003	R = 0.37 *P* = 0.15	R = 0.26 *P* = 0.33	R = 0.33 *P* = 0.21	R = 0.32 *P* = 0.22
Uridine triphosphate	R = -0.47 *P* = 6.3e-02	R = -0.35 *P* = 0.17	R = -0.30 *P* = 0.26	R = -0.39 *P* = 0.13	R = -0.10 *P* = 0.72	R = -0.21 *P* = 0.42	R = -0.33 *P* = 0.21	R = -0.19 *P* = 0.48	R = 0.42 *P* = 0.10	R = 0.43 *P* = 0.09	R = 0.33 *P* = 0.20	R = -0.13 *P* = 0.63	R = 0.10 *P* = 0.72	R = 0.28 *P* = 0.28

	Akkermansia muciniphila	Lachnospiraceae bacterium_DW59	Bacteroides caecimuris	Clostridiales Bacterium CIEAF_020	Aerococcus urinaeequi	Burkholderiales Bacterium YL45	Clostridium leptum	Clostridium sp Clone.44	Proteus vulgaris	Mucispirillum schaedleri	Klebsiella oxytoca	Lactobacillus murinus	Enterococcus casseliflavus	Citrobacter freundii
Vitamin D3	R = 0.64 *P* = 6.9e-03	R = 0.43 *P* = 0.09	R = 0.54 *P* = 0.03	R = 0.31 *P* = 0.24	R = 0.40 *P* = 0.13	R = 0.54 *P* = 0.03	R = 0.42 *P* = 0.11	R = 0.40 *P* = 0.13	R = -0.37 *P* = 0.16	R = -0.63 *P* = 0.009	R = -0.27 *P* = 0.31	R = -0.11 *P* = 0.69	R = -0.17 *P* = 0.51	R = -0.23 *P* = 0.39
5,6-dehydroarachidonic acid	R = 0.56 *P* = 2.3e-02	R = 0.40 *P* = 0.12	R = 0.55 *P* = 0.03	R = 0.34 *P* = 0.19	R = 0.11 *P* = 0.67	R = 0.44 *P* = 0.08	R = 0.20 *P* = 0.45	R = 0.39 *P* = 0.13	R = -0.53 *P* = 0.04	R = -0.43 *P* = 0.09	R = -0.49 *P* = 0.06	R = -0.14 *P* = 0.61	R = -0.33 *P* = 0.21	R = -0.37 *P* = 0.15
B-Pseudouridine	R = 0.63 *P* = 7.9e-03	R = 0.45 *P* = 0.08	R = 0.40 *P* = 0.12	R = 0.54 *P* = 0.03	R = 0.24 *P* = 0.37	R = 0.41 *P* = 0.11	R = 0.53 *P* = 0.03	R = 0.44 *P* = 0.08	R = -0.36 *P* = 0.16	R = -0.67 *P* = 0.004	R = -0.22 *P* = 0.41	R = -0.003 *P* = 0.99	R = -0.12 *P* = 0.67	R = -0.15 *P* = 0.56
4-Hydroxyphenylpyruvic Acid	R = 0.54 *P* = 2.8e-02	R = 0.22 *P* = 0.40	R = 0.36 *P* = 0.17	R = 0.49 *P* = 0.06	R = 0.31 *P* = 0.23	R = 0.52 *P* = 0.04	R = 0.41 *P* = 0.11	R = 0.28 *P* = 0.29	R = -0.27 *P* = 0.31	R = -0.74 *P* = 0.002	R = -0.16 *P* = 0.55	R = 0.13 *P* = 0.63	R = 0.01 *P* = 0.96	R = -0.17 *P* = 0.54
Alanine tyrosine	R = 0.49 *P* = 4.9e-02	R = 0.52 *P* = 0.04	R = 0.50 *P* = 0.04	R = 0.58 *P* = 0.02	R = 0.24 *P* = 0.37	R = 0.38 *P* = 0.14	R = 0.55 *P* = 0.02	R = 0.49 *P* = 0.06	R = -0.38 *P* = 0.14	R = -0.70 *P* = 0.003	R = -0.31 *P* = 0.24	R = -0.20 *P* = 0.44	R = -0.22 *P* = 0.40	R = -0.27 *P* = 0.31
A-Ketoglutaric Acid	R = 0.57 *P* = 2e-02	R = 0.40 *P* = 0.12	R = 0.39 *P* = 0.13	R = 0.58 *P* = 0.02	R = 0.28 *P* = 0.28	R = 0.49 *P* = 0.06	R = 0.46 *P* = 0.07	R = 0.48 *P* = 0.06	R = -0.48 *P* = 0.06	R = -0.78 *P* = 0.0004	R = -0.40 *P* = 0.13	R = -0.14 *P* = 0.59	R = -0.21 *P* = 0.44	R = -0.38 *P* = 0.14
Malonicacid	R = 0.90 *P* = 1.9e-06	R = 0.68 *P* = 0.003	R = 0.60 *P* = 0.02	R = 0.53 *P* = 0.03	R = 0.34 *P* = 0.19	R = 0.72 *P* = 0.002	R = 0.51 *P* = 0.04	R = 0.80 *P* = 0.0002	R = -0.65 *P* = 0.006	R = -0.74 *P* = 0.0009	R = -0.66 *P* = 0.005	R = -0.30 *P* = 0.25	R = -0.64 *P* = 0.007	R = -0.61 *P* = 0.02
3-Hydroxybutyrate	R = 0.92 *P* = 5.2e-07	R = 0.72 *P* = 0.002	R = 0.63 *P* = 0.008	R = 0.57 *P* = 0.02	R = 0.36 *P* = 0.17	R = 0.70 *P* = 0.003	R = 0.50 *P* = 0.04	R = 0.75 *P* = 0.0008	R = -0.68 *P* = 0.004	R = -0.76 *P* = 0.0006	R = -0.68 *P* = 0.003	R = -0.29 *P* = 0.27	R = -0.63 *P* = 0.008	R = -0.66 *P* = 0.005
Indole-2-Carboxylic Acid	R = 0.53 *P* = 3e-02	R = 0.52 *P* = 0.04	R = 0.35 *P* = 0.19	R = 0.57 *P* = 0.02	R = -0.04 *P* = 0.88	R = 0.25 *P* = 0.35	R = 0.65 *P* = 0.007	R = 0.50 *P* = 0.04	R = -0.31 *P* = 0.24	R = -0.53 *P* = 0.03	R = -0.28 *P* = 0.29	R = -0.06 *P* = 0.82	R = -0.21 *P* = 0.43	R = -0.25 *P* = 0.35
Tryptamine	R = 0.50 *P* = 4.7e-02	R = 0.43 *P* = 0.09	R = 0.34 *P* = 0.19	R = 0.60 *P* = 0.02	R = -0.005 *P* = 0.98	R = 0.27 *P* = 0.30	R = 0.59 *P* = 0.02	R = 0.46 *P* = 0.07	R = -0.25 *P* = 0.35	R = -0.59 *P* = 0.02	R = -0.16 *P* = 0.55	R = 0.03 *P* = 0.91	R = -0.11 *P* = 0.67	R = -0.10 *P* = 0.70

Table S7. The details of correlation between selected differential bacteria in WT and RP mice.

Spearman correlation between selected differential bacteria in WT and RP mice.

	Akkermansia muciniphila	**Lachnospiraceae bacterium_DW59**	**Bacteroides caecimuris**	**Clostridiales Bacterium CIEAF_020**	**Aerococcus urinaeequi**	**Burkholderiales Bacterium YL45**	**Clostridium leptum**	**Clostridium sp Clone.44**	**Proteus vulgaris**	**Mucispirillum schaedleri**	**Klebsiella oxytoca**	**Lactobacillus murinus**	**Enterococcus casseliflavus**	**Citrobacter freundii**
Akkermansia muciniphila		R =0.70 *P* = 0.003	R = 0.57 *P* = 0.022	R = 0.45 *P* = 0.080	R = 0.25 *P* = 0.338	R = 0.67 *P* = 0.005	R = 0.47 *P* = 0.064	R = 0.67 *P* = 0.005	R = -0.61 *P* = 0.013	R = -0.57 *P* = 0.022	R = -0.63 *P* = 0.009	R = -0.08 *P* = 0.766	R = -0.57 *P* = 0.022	R = -0.61 *P* = 0.012
Lachnospiraceae bacterium_DW59	R = 0.70 *P* = 0.003		R = 0.63 *P* = 0.009	R = 0.55 *P* = 0.027	R = 0.46 *P* = 0.071	R = 0.39 *P* = 0.131	R = 0.56 *P* = 0.024	R = 0.64 *P* = 0.007	R = -0.60 *P* = 0.015	R = -0.34 *P* = 0.196	R = -0.62 *P* = 0.009	R = -0.49 *P* = 0.052	R = -0.54 *P* = 0.030	R = -0.53 *P* = 0.036
Bacteroides caecimuris	R = 0.57 *P* = 0.022	R = 0.63 *P* = 0.009		R = 0.46 *P* = 0.076	R = 0.51 *P* = 0.046	R = 0.72 *P* = 0.002	R = 0.28 *P* = 0.290	R = 0.36 *P* = 0.167	R = -0.38 *P* = 0.141	R = -0.35 *P* = 0.180	R = -0.47 *P* = 0.068	R = -0.44 *P* = 0.088	R = -0.31 *P* = 0.247	R = -0.40 *P* = 0.124
Clostridiales Bacterium CIEAF_020	R = 0.45 *P* = 0.080	R = 0.55 *P* = 0.027	R = 0.46 *P* = 0.076		R = 0.12 *P* = 0.650	R = 0.46 *P* = 0.075	R = 0.59 *P* = 0.017	R = 0.53 *P* = 0.034	R = -0.22 *P* = 0.401	R = -0.57 *P* = 0.021	R = -0.29 *P* = 0.283	R = -0.22 *P* = 0.409	R = -0.08 *P* = 0.754	R = -0.26 *P* = 0.337
Aerococcus urinaeequi	R = 0.25 *P* = 0.338	R = 0.46 *P* = 0.071	R = 0.51 *P* = 0.046	R = 0.12 *P* = 0.650		R = 0.47 *P* = 0.065	R = 0.28 *P* = 0.285	R = 0.02 *P* = 0.929	R = -0.21 *P* = 0.430	R = -0.19 *P* = 0.477	R = -0.20 *P* = 0.454	R = -0.34 *P* = 0.191	R = -0.02 *P* = 0.938	R = -0.09 *P* = 0.737
Burkholderiales Bacterium YL45	R = 0.67 *P* = 0.005	R = 0.39 *P* = 0.131	R = 0.72 *P* = 0.002	R = 0.46 *P* = 0.075	R = 0.47 *P* = 0.065		R = 0.27 *P* = 0.316	R = 0.50 *P* = 0.048	R = -0.23 *P* = 0.383	R = -0.42 *P* = 0.101	R = -0.41 *P* = 0.119	R = -0.18 *P* = 0.503	R =-0.21 *P* = 0.431	R = -0.34 *P* = 0.201
Clostridium leptum	R = 0.47 *P* = 0.064	R = 0.56 *P* = 0.024	R = 0.28 *P* = 0.290	R = 0.59 *P* = 0.017	R = 0.28 *P* = 0.285	R = 0.27 *P* = 0.316		R = 0.47 *P* = 0.065	R = -0.17 *P* = 0.529	R = -0.47 *P* = 0.067	R = -0.16 *P* = 0.558	R = -0.34 *P* = 0.199	R = -0.12 *P* = 0.652	R = -0.09 *P* = 0.736
Clostridium sp Clone.44	R = 0.67 *P* = 0.005	R = 0.64 *P* = 0.007	R = 0.36 *P* = 0.167	R = 0.53 *P* = 0.034	R = 0.02 *P* = 0.929	R = 0.50 *P* = 0.048	R = 0.47 *P* = 0.065		R = -0.51 *P* = 0.043	R = -0.48 *P* = 0.059	R = -0.56 *P* = 0.024	R = -0.38 *P* = 0.144	R = -0.63 *P* = 0.009	R = -0.48 *P* = 0.059
Proteus vulgaris	R = -0.61 *P* = 0.013	R = -0.60 *P* = 0.015	R = -0.38 *P* = 0.141	R = -0.22 *P* = 0.401	R = -0.21 *P* = 0.430	R = -0.23 *P* = 0.383	R = -0.17 *P* = 0.529	R = -0.51 *P* = 0.043		R = 0.53 *P* = 0.033	R = 0.92 *P* = 3e-07	R = 0.22 *P* = 0.403	R = 0.83 *P* = 6e-05	R = 0.89 *P* = 4e-06
Mucispirillum schaedleri	R = -0.57 *P* = 0.022	R = -0.34 *P* = 0.196	R = -0.35 *P* = 0.180	R = -0.57 *P* = 0.021	R = -0.19 *P* = 0.477	R = -0.42 *P* = 0.101	R = -0.47 *P* = 0.067	R = -0.48 *P* = 0.059	R = 0.53 *P* = 0.033		R = 0.42 *P* = 0.108	R = 0.10 *P* = 0.697	R = 0.37 *P* = 0.163	R = 0.50 *P* = 0.047
Klebsiella oxytoca	R = -0.63 *P* = 0.009	R = -0.62 *P* = 0.009	R = -0.47 *P* = 0.068	R = -0.29 *P* = 0.283	R = -0.20 *P* = 0.454	R = -0.40 *P* = 0.119	R = -0.16 *P* = 0.558	R = -0.56 *P* = 0.024	R = 0.92 *P* = 3e-07	R = 0.42 *P* = 0.108		R = 0.32 *P* = 0.232	R = 0.86 *P* = 1e-05	R = 0.94 *P* = 5e-08
Lactobacillus murinus	R = -0.08 *P* = 0.766	R = -0.49 *P* = 0.052	R = -0.44 *P* = 0.088	R = -0.22 *P* = 0.409	R = -0.34 *P* = 0.191	R = -0.18 *P* = 0.503	R = -0.34 *P* = 0.199	R = -0.38 *P* = 0.144	R = 0.22 *P* = 0.403	R = 0.10 *P* = 0.697	R = 0.32 *P* = 0.232		R = 0.35 *P* = 0.182	R = 0.24 *P* = 0.361
Enterococcus casseliflavus	R = -0.57 *P* = 0.022	R = -0.54 *P* = 0.030	R = -0.31 *P* = 0.247	R = -0.08 *P* = 0.754	R = -0.02 *P* = 0.938	R = -0.21 *P* = 0.431	R = -0.12 *P* = 0.652	R = -0.63 *P* = 0.009	R = 0.83 *P* = 6e-05	R = 0.37 *P* = 0.163	R = 0.86 *P* = 1e-05	R = 0.35 *P* = 0.182		R = 0.82 *P* = 1e-04
Citrobacter freundii	R = -0.61 *P* = 0.012	R = -0.53 *P* = 0.036	R = -0.40 *P* = 0.124	R = -0.26 *P* = 0.337	R = -0.09 *P* = 0.737	R = -0.34 *P* = 0.201	R = -0.09 *P* = 0.736	R = -0.48 *P* = 0.059	R = 0.89 *P* = 4e-06	R = 0.50 *P* = 0.047	R = 0.94 *P* = 5e-08	R = 0.24 *P* = 0.361	R = 0.82 *P* = 1e-04	

Table S8. **The details of correlation between bacteria and cytokine concentration measured in the RP mice.**

Spearman correlation between bacteria and cytokine concentration measured in the RP mice.

	IL1β	IL2	IL4	IL5	IL6	TNFα
Akkermansia_muciniphila	R = 0.49 *P* = 0.22	R = 0.32 *P* = 0.43	R = -0.35 *P* = 0.39	R = 0.15 *P* = 0.71	R = -0.88 *P* = 0.003	R = 0.32 *P* =0.43
Lachnospiraceae_bacterium_DW59	R = 0.62 *P* = 0.10	R = -0.19 *P* = 0.65	R = -0.32 *P* = 0.43	R = 0.14 *P* = 0.73	R = -0.67 *P* = 0.07	R = 0.19 *P* = 0.65
Bacteroides_caecimuris	R = 0.52 *P* = 0.18	R = 0.62 *P* = 0.10	R = -0.31 *P* = 0.45	R = -0.26 *P* = 0.53	R = -0.38 *P* = 0.35	R = 0.69 *P* = 0.058
Clostridiales_bacterium_CIEAF_020	R = 0.25 *P* = 0.55	R = -0.22 *P* = 0.59	R = -0.52 *P* = 0.19	R = -0.86 *P* = 0.006	R = 0.14 *P* = 0.73	R = 0.33 *P* = 0.42
Aerococcus_urinaeequi	R = 0.38 *P* = 0.35	R = -0.38 *P* = 0.35	R = -0.06 *P* = 0.88	R = -0.25 *P* = 0.55	R = 0.12 *P* = 0.77	R = 0.25 *P* = 0.55
Burkholderiales_bacterium_YL45	R = 0.39 *P* = 0.33	R = 0.47 *P* = 0.24	R = -0.17 *P* = 0.69	R = -0.59 *P* = 0.13	R = -0.13 *P* = 0.75	R = 0.71 *P* = 0.051
Clostridium._leptum	R = -0.01 *P* = 0.98	R = -0.18 *P* = 0.66	R = -0.17 *P* = 0.69	R = -0.44 *P* = 0.27	R = -0.20 *P* = 0.64	R = -0.05 *P* = 0.91
Clostridium_sp_Clone.44	R = -0.44 *P* = 0.28	R = 0.39 *P* = 0.34	R = 0.56 *P* = 0.14	R = 0.10 *P* = 0.82	R = -0.22 *P* = 0.60	R = -0.05 *P* = 0.91
Proteus_vulgaris	R = -0.17 *P* = 0.69	R = -0.50 *P* = 0.21	R = -0.01 *P* = 0.98	R = -0.67 *P* = 0.07	R = 0.48 *P* = 0.23	R = -0.05 *P* = 0.91
Mucispirillum_schaedleri	R = 0.14 *P* = 0.73	R = -0.24 *P* = 0.57	R = 0.35 *P* = 0.40	R = -0.14 *P* = 0.73	R = 0.21 *P* = 0.61	R = 0.05 *P* = 0.91
Klebsiella_oxytoca	R = -0.40 *P* = 0.32	R = -0.74 *P* = 0.04	R = 0.13 *P* = 0.75	R = -0.43 *P* = 0.29	R = 0.48 *P* = 0.23	R = -0.43 *P* = 0.29
Lactobacillus_murinus	R = 0.28 *P* = 0.49	R = 0 *P* = 1.00	R = 0.15 *P* = 0.71	R = 0.17 *P* = 0.69	R = 0.21 *P* = 0.61	R = 0.02 *P* = 0.95
Enterococcus_casseliflavus	R = 0.31 *P* = 0.45	R = -0.26 *P* = 0.53	R = -0.32 *P* = 0.43	R = -0.57 *P* = 0.14	R = 0.59 *P* = 0.12	R = 0.24 *P* = 0.57
Citrobacter_freundii	R = -0.52 *P* = 0.18	R = -0.86 *P* = 0.006	R = 0.38 *P* = 0.35	R = -0.31 *P* = 0.45	R = 0.40 *P* = 0.32	R = -0.55 *P* = 0.16

Table S9. Information of oncology patients

Patients	Sex	Age	Height/cm	Weight/kg	Disease	Medicine[a]	Radiotherapy treatment
#1	Female	46	164	60	Rectal cancer	folfox + PD-1	PTV-GTV 50Gy/25F, PTV-CTV 45Gy/25F
#2	Female	54	160	72	Rectal cancer	folfox	PTV-GTV 50Gy/25F, PTV-CTV 45Gy/25F
#3	Female	60	159	55	Rectal cancer	folfox	PTV-GTV 50Gy/25F, PTV-CTV 45Gy/25F
#4	Female	34	159	44	Rectal cancer	folfox	PTV-GTV 50Gy/25F, PTV-CTV 45Gy/25F
#5	Male	55	165	65	Rectal cancer	folfox	PTV-GTV 50Gy/25F, PTV-CTV 45Gy/25F
#6	Male	53	163	64	Rectal cancer	folfox	PTV-GTV 50Gy/25F, PTV-CTV 45Gy/25F
#7	Male	64	165	63	Rectal cancer	folfox + PD-1	PTV-GTV 50Gy/25F, PTV-CTV 45Gy/25F

a. folfox: Oxaliplatin, Calcium levovorin and Fluorouracil.

Table S10. The primers used in this study.

V3-V4	forward primer 5′-ACTCCTACGGGAGGCAGCA-3′
	reverse primer 5′-GGACTACHVGGGTWTCTAAT-3′
A. muciniphila	forward primer 5′-CAGCACGTGAAGGTGGGGAC-3′
	reverse primer 5′-CCTTGCGGTTGGCTTCAGAT-3′
16S rDNA	forward primer 5′-CGGTGAATACGTTCCCGG-3′
	reverse primer 5′-TACGGCTACCTTGTTACGACTT-3′
q-mGPR43	forward primer 5′-TTGAGCAAGCGGTGGTGAAG-3′
	reverse primer 5′-GGGAGCCCAGTAAGAAAGATGAG-3′
q-mGPR41	forward primer 5′-GCAGCAGAGTGCCAGTTGTCC-3′
	reverse primer 5′-CTTGCCCACGAAGACCACC-3′
q-mGPR40	forward primer 5′-TCTCCTTCGCTCTCTATGTATCTGC-3′
	reverse primer 5′-GAGTCGCAGTTTAGCGTGGGA-3′
q-mGPR109A	forward primer 5′-GTTCGGACTCCTGGGCAATG-3′
	reverse primer 5′-GTCAGGAACGGCAGGCAGAT-3′
q-mGPR81	forward primer 5′-CGCAGAGCGTGAGGGAAAA-3′
	reverse primer 5′-CGTCCCCTACAGAGTTGAAGCCT-3′
q-mGPR35	forward primer 5′-GCACAGTCGCTCCACTTACAGG-3′
	reverse primer 5′-GACCCCAGTCCAGCCTCATTC-3′
q-mIL6	forward primer 5′-GGAGCCCACCAAGAACGATAG-3′
	reverse primer 5′-CCAGCATCAGTCCCAAGAAGG-3′
q-mGAPDH	forward primer 5′-GAGAGTGTTTCCTCGTCCCGTAG-3′
	reverse primer 5′-CAACAATCTCCACTTTGCCACTG-3′
q-hGPR43	forward primer 5′-CCCTCACGAGTTTTGGCTTCTAC-3′
	reverse primer 5′-GCAGTGACCAAAGGACATAACCC-3′
q-hIL6	forward primer 5-′TGTGTGAAAGCAGCAAAGAGGC-3′
	reverse primer 5′-GATGATTTTCACCAGGCAAGTCTC-3′
q-hGAPDH	forward primer 5′-GCGGGGCTCTCCAGAACATC-3′
	reverse primer 5′-GCAGTGGGGACACGGAAGG-3′
p-FabG	forward primer 5′-ATGCAAAAGTTAGCAGGTAA-3′
	reverse primer 5′-CTACATCGTCATGCCTCCGT-3′
q-FabG mRNA	forward primer 5′-ATGAAAGAGGAAGACTGGGATGC-3′
	reverse primer 5′-CGATGTTGCCGACGAGACC-3′